# Aerodynamics <span style="float:right">12</span>

Flows past airplane wings and high-speed ground vehicles has captured the attention of fluid dynamicists, applied mathematicians, and computational scientists and engineers, not only because of their obvious technological significance, but also because of the opportunity they present to perform elegant mathematical analysis and develop realistic and efficient numerical models. Although these flows occur at high Reynolds numbers and often at transonic or supersonic speeds that are comparable to, or even exceed the speed of sound, the effect of viscosity is important in two ways. First, viscous stresses determine the drag force exerted on moving surfaces and thus the energy required to sustain the motion. Second, viscous stresses are responsible for production of vorticity which generates circulation and thereby induces a lift force.

A comprehensive analysis of high-speed flow in aerodynamics incorporates the effects of fluid compressibility and turbulent motion, and accounts for the presence of boundary layers and regions of recirculating flow. In this chapter, we discuss the most basic configuration that arises by neglecting the presence of boundary layers and wakes, and by assuming that the fluid is inviscid and incompressible. The simplified model involving irrotational flow in the presence of global circulatory motion is amenable to efficient numerical methods that illustrate the importance of computational fluid dynamics in the practical field of aerodynamics.

## 12.1   General features of flow past an aircraft

A schematic illustration of flow past an aircraft that has taken off and traveled by a certain distance is shown in Figure 12.1.1 in a frame of reference moving with the aircraft. If the flow is subsonic, the following features are most significant:

- A thin vortex loop resembling a line vortex is established behind the aircraft. The loop
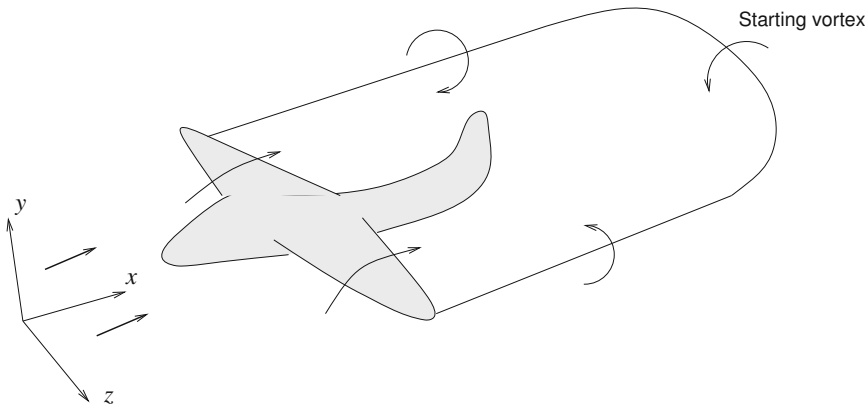
**Figure 12.1.1**   Schematic illustration of flow past an aircraft in a frame of reference moving with the aircraft.

extends from the left wing tip, back at a length that is comparable to the distance that the aircraft has traveled, and then forward to the right wing tip. The trailing vortex at the back of the loop was generated when the airplane first started moving, and is accordingly called the starting vortex. The vortex loop can be extended artificially into the wings to form a closed line vortex.

The circulation around any closed loop that encloses the line vortex is constant, independent of the shape and location of the loop. Thus, the circulation around a simple loop that encloses a wing is equal to the circulation around a simple loop that encloses the trailing vortex.

- Viscous stresses cause the vortex loop to diffuse and its vortex core to be smeared. However, the circulation around any loop that encloses the smeared vortex loop is equal to the circulation around a loop that encloses a wing, no matter how far the vorticity has spread out.

- The circulation around a loop that encloses a wing is determined by the speed of the aircraft and the geometry and orientation of the wings with respect to the incoming wind, as discussed in Section 12.2.

- If the aircraft suddenly changes its speed or direction of flight, a new vortex loop will be ejected, contributing an additional amount of circulation around the wings.

- Each wing experiences a lift force normal to the direction of flight, and a drag force parallel to the direction of flight. The later must be compensated by the thrust produced by the engine.

The lift force can be computed with surprising accuracy by neglecting the effects of viscosity and assuming that the flow around the airfoil is irrotational. To compute the drag
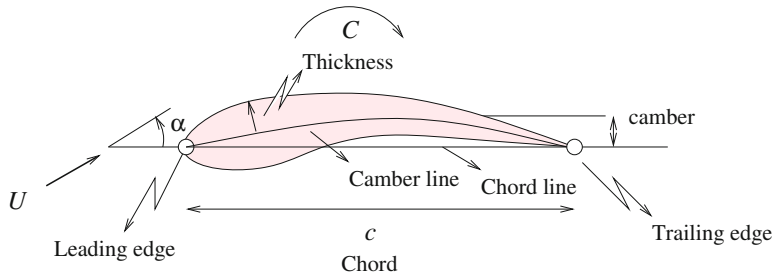
**Figure 12.2.1** Illustration of an airfoil and its standard geometrical properties, also showing the angle of attack, $\alpha$.

force, we must carry out a boundary-layer analysis of the basic irrotational flow, as discussed in Chapter 10.

It is important to bear in mind that the main features of the flow past an aircraft discussed in this chapter assume that the wings are only slightly tilted with respect to the direction of the incoming wind. When this condition is not met, large regions of recirculating flow may develop over the upper surface of the airfoil, seriously affecting the structure of the flow and performance of the aircraft.

To study the flow past the wings and compute the lift force per unit span exerted on them, we may assume that the flow is locally two-dimensional occurring in the $xy$ plane that is normal to the line connecting the wing tips. It turns out that neglecting the third dimension provides us with a theoretical model whose predictions are in good and sometimes excellent agreement with laboratory measurements taken in wind tunnels. In the remainder of this chapter, we concentrate on the two-dimensional flow. The three-dimensional flow is an advanced topic suitable for a second course in aerodynamics.

## 12.2  Airfoils and the Kutta–Joukowski condition

An airfoil is a section of a wing, as shown in Figure 12.2.1. The shape of an airfoil is determined by the following geometrical parameters:

- The *chord line*, defined as the straight line connecting the leading edge to the trailing edge.

- The *chord*, defined as the distance from the leading edge to the trailing edge.

- The *camber line*, defined as the locus of points located halfway between the upper and lower surface of the airfoil.

- The *camber*, defined as the maximum displacement of the camber line from the chord line. The camber of a symmetric airfoil is zero.

- The *airfoil thickness* along the camber line.

The angle subtended between the incoming wind and the chord line, $\alpha$, is the *angle of attack*, as shown in Figure 12.2.1.

### NACA airfoils

The National Advisory Committee for Aeronautics of the United States (NACA), the predecessor of today's NASA, has standardized airfoil shapes to facilitate engineering design. NACA airfoils are generated by specifying the geometry of the camber line, and then wrapping around the camber line an airfoil contour to obtain a desired distribution of half-thickness.

The dated four-digit NACA *mnlk* airfoils, where $m, n, k, l$ are four integers, have a camber of $0.0m \times c$, occurring at a distance $0.0n \times c$ from the leading edge, where $c$ is the chord. The maximum airfoil thickness is $0.kl \times c$.

The following MATLAB code entitled *NACA4*, located in directory *airf_2d* inside directory *07_ptf* of FDLIB, generates a four-digit NACA airfoil:

```
chord = 1.0;
xcam = 0.4;
cam = 0.05;
thick = 0.1;

n = 32;   % number of nodes around the airfoil

%----
% prepare
%----

dpsi = 2*pi/n;

%----
% prepare to plot
%----

figure(1)
hold on
axis equal
xlabel('x','fontsize',13)
ylabel('y','fontsize',13)

%----
% run over nodes
%----

for i=1:n
  psi = (i-1.0)*dpsi;
  x = 0.5*(1.0+cos(psi));
```

```
% camber line:

if(x<xcam)
  yc(i) = cam*(2.0*xcam*x-x*x)/xcam^2;
else
  yc(i) = cam/(1.0-xcam)^2 ...
    *((1.0-2.0*xcam)+2.0*xcam*x-x*x);
end

% thickness:

yt = 5.0*thick *(0.2969*sqrt(x) -0.1260*x...
  -0.3516*x*x +0.2843*x*x*x -0.1036*x*x*x*x );

% contour:

if(i<(n/2+1))
  ya(i) = (yc(i)-yt)*chord;
else
  ya(i) = (yc(i)+yt)*chord;
end

xa(i) = x*chord;

end

xa(n+1) = chord;
ya(n+1) = 0.0;
yc(n+1) = 0.0;   % trailing edge

%----
% plot
%----

plot(xa,ya,'ko-');
plot(xa,yc,'k--');
```

The graphics display generated by the code is shown in Figure 12.2.2.

Modern five- and six-digit airfoils are encoded with additional geometrical and flow properties.

*Airfoil shapes by mapping*

Airfoil shapes can be generated by mapping a closed contour in an auxiliary parametric $(\xi, \eta)$ plane to the airfoil contour in the physical $xy$ plane using an appropriate mapping function. In theoretical aerodynamics, the mapping function arises from a function of a
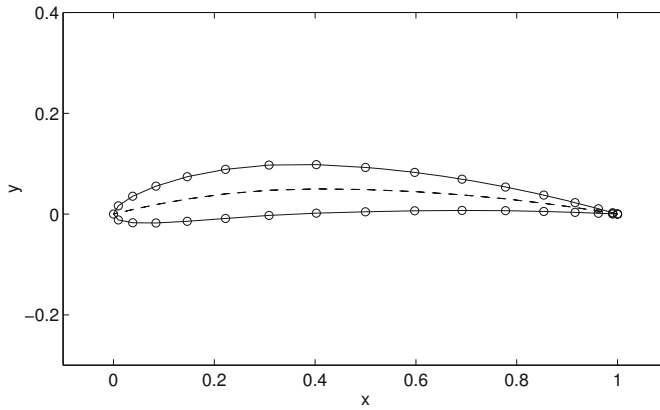
**Figure 12.2.2**   Contour of a four-digit NACA airfoil generated by a MATLAB program named NACA4.

complex variable, $f(\zeta)$, by setting

$$z = f(\zeta), \tag{12.2.1}$$

where

$$z \equiv x + \mathrm{i}\, y, \qquad \zeta \equiv \xi + \mathrm{i}\, \eta \tag{12.2.2}$$

are two complex variables, and i is the imaginary unit satisfying $\mathrm{i}^2 = -1$.

### Joukowski's transformation

Joukowski's transformation employs the mapping function

$$f(\zeta) = \zeta + \frac{\sigma^2}{\zeta}, \tag{12.2.3}$$

where $\sigma$ is a specified length. A circle in the $\xi\eta$ plane passing through the singular point $(-\sigma, 0)$ and enclosing the reflected singular point $(\sigma, 0)$ is mapped to a cusped airfoil whose camberline and camber are determined by the location of the center of the circle in the $\xi\eta$ plane, as shown in Figure 12.2.3. The airfoil cusp is located at the image of the first singular point. Different airfoil shapes can be generated by fixing the value of $\sigma$ and varying the position of the center of the circle, $\mathbf{x}_c$, in the $\xi\eta$ plane.

The following MATLAB code entitled *joukowski,* located in directory *airf_2d* inside directory *07_ptf* of FDLIB, generates airfoil shapes:
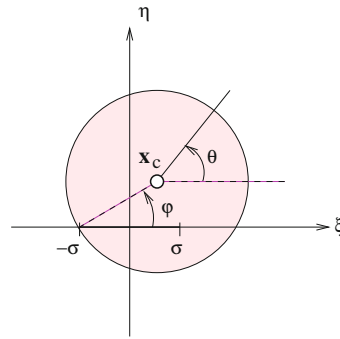
**Figure 12.2.3**   A Joukowski airfoil is generated by mapping conformally a circle in the $\xi\eta$ plane to an airfoil contour in the $xy$ plane. The first singular point, located at the $\xi$ axis at $\xi = -\sigma$, is mapped to the airfoil trailing edge. The second singular point, located at $\xi = \sigma$, is mapped inside the airfoil.

```
xc = 0.1;  % circle center
yc = 0.2;   % circle center
n = 32;      % number of contour nodes
sigma = 1.0;

%---
% prepare
%---

radius = sqrt((xc+sigma)^2+yc*yc);
phi = acos((xc+sigma)/radius);
thstart = -pi+phi;
dth = 2*pi/n;

%---
% run around the airfoil
%---

for i=1:n+1
   th = thstart+(i-1)*dth;
   xi = xc+radius*cos(th);
   et = yc+radius*sin(th);
   r2 = xi*xi+et*et;
   x(i) = xi*(1.0+sigma^2/r2);
   y(i) = et*(1.0-sigma^2/r2);
end

%---
% plot
%---
```
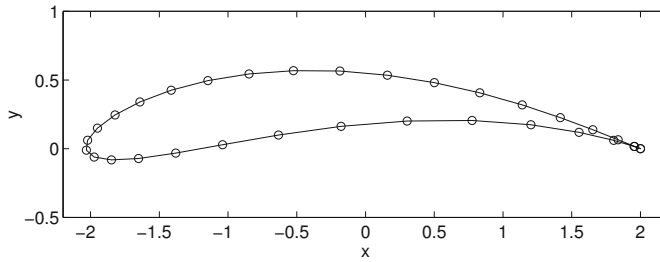
**Figure 12.2.4**  A Joukowski airfoil generated by the code joukowski listed in the text for the parameter values listed in the code.

```
plot(-x,y,'o-')
axis equal
xlabel('x','fontsize',13)
ylabel('y','fontsize',13)
```

The graphics display generated by the code is shown in Figure 12.2.4. Note that the starting angle $\phi$ is defined in Figure 12.2.3. The first and last points, labeled 1 and $n+1$ are mapped to the trailing edge. Intermediate points are distributed in the counterclockwise direction around the airfoil. Note that the airfoil contour has been reflected at the plotting stage to place the leading edge on the left.

### 12.2.1   The Kutta–Joukowski theorem

The lift force per unit span exerted on an airfoil, $L$, is determined by the incoming wind speed, $U$, and by the circulation of the fluid around the airfoil, $C$, as determined by the Kutta–Joukowski theorem expressed by the equation

$$L = -\rho U C, \tag{12.2.4}$$

where $\rho$ is the density of the fluid. Note that positive lift, $L > 0$, requires negative circulation associated with clockwise rotation around the airfoil, $C < 0$ as illustrated in Figure 12.2.1. If the circulation vanishes, the lift force is zero.

The Kutta–Joukowski theorem can be proved most readily working under the auspices of analytic function theory in complex variables, as discussed in the texts cited in the bibliography.

#### Flow past a cylinder

To confirm the Kutta–Joukowski theorem, we consider streaming (uniform) flow past a circular cylinder of radius $a$ discussed in Section 3.7. Applying Bernoulli's equation (6.4.18) at infinity and at a point on the surface of the cylinder, and evaluating the tangential velocity on the surface of the cylinder using formula (3.7.10), we derive an expression for the surface

pressure,

$$p_{r=a} = -2\rho \, V_x^2 \, (\sin\theta + \beta)^2 + p_\infty, \tag{12.2.5}$$

where $p_\infty$ is the pressure at infinity, $\beta$ is a dimensionless circulation parameter defined in equation (3.7.9) as

$$\beta \equiv -\frac{C}{4\pi V_x \, a}, \tag{12.2.6}$$

and $C$ is the circulation around the cylinder.

In the absence of viscous stresses, the force per unit span exerted on the cylinder is given by

$$\mathbf{F} = \oint \big[ -p_{r=a} \big] \, \mathbf{n} \, d\ell = - \int_0^{2\pi} p_{r=a} \, \mathbf{n} \, a \, d\theta, \tag{12.2.7}$$

where $d\ell = a \, d\theta$ is the differential arc length around the cylinder and $\mathbf{n} = (\cos\theta, \sin\theta)$ is the unit vector normal to the cylinder pointing into the fluid. Substituting the pressure distribution (12.2.5) into (12.2.7), we find that the $x$ component of the force vanishes, while the $y$ component of the force is given by

$$F_y \equiv L = 2\rho \, a \, V_x^2 \int_0^{2\pi} (\sin\theta + \beta)^2 \, \sin\theta \, a \, d\theta. \tag{12.2.8}$$

Performing the integration, we obtain

$$L = 4\pi a \rho V_x^2 \beta. \tag{12.2.9}$$

Recalling the definition of $\beta$ given in (12.2.6), we find that

$$L = -\rho \, V_x \, C, \tag{12.2.10}$$

which is consistent with the Kutta–Joukowski theorem expressed by (12.2.4).

### 12.2.2   The Kutta–Joukowski condition

In the context of irrotational flow theory, the circulation around an airfoil, or any two-dimensional body, is arbitrary. Kutta and Joukowski observed independently that, in practice, when the angle of attack $\alpha$ is sufficiently small, the flow on the upper side of an airfoil joins smoothly with the flow on the lower side of the airfoil at the trailing edge. This observation provides us with a physical basis for the Kutta–Joukowski condition stipulating that the circulation established around an airfoil is such that a singular flow does not arise at the trailing edge, and therefore the fluid does not have to turn around a cornered or cusped trailing edge.

Referring to the Kutta–Joukowski theorem expressed by (12.2.4), we see that a well-designed airfoil should be able to generate a high degree of circulation, while minimizing the drag force exerted on the airfoil.

**Problems**

**12.2.1** *Flow past a cylinder*

Carry out the integration in (12.2.7) with the pressure given in (12.2.5) to derive expression (12.2.10).

**12.2.2** 🖳 *Joukowski airfoils*

Run the code *joukowski* to generate several airfoil shapes of your choice. Investigate the effect of the location of the mapped circle center.

## 12.3   Vortex panels

We begin the study of two-dimensional flow past an airfoil by introducing a class of elementary flows associated with vortex panels. Our ultimate objective is to use these elementary flows as fundamental building blocks for describing the flow past an airfoil with arbitrary shape, where the circulation around the airfoil is determined by the Kutta–Joukowski condition discussed in Section 12.2.2.

### Flow due to a point vortex

In Section 3.7, we introduced the two-dimensional irrotational flow with circulatory motion induced by a point vortex. The $x$ and $y$ components of the velocity at a point, $\mathbf{x} = (x, y)$, due to a point vortex with strength $\kappa$ located at another point, $\mathbf{x}_0 = (x_0, y_0)$, were given in equations (11.2.1) and (11.2.2), repeated below for convenience,

$$u_x(x, y) = -\frac{\kappa}{2\pi} \frac{y - y_0}{(x - x_0)^2 + (x - y_0)^2} \tag{12.3.1}$$

and

$$u_y(x, y) = \frac{\kappa}{2\pi} \frac{x - x_0}{(x - x_0)^2 + (x - y_0)^2}. \tag{12.3.2}$$

The associated stream function is given by

$$\psi(x, y) = -\frac{\kappa}{4\pi} \ln \frac{(x - x_0)^2 + (y - y_0)^2}{\varrho^2}, \tag{12.3.3}$$

where $\varrho$ is an arbitrary constant length. The corresponding multi-valued velocity potential is given by

$$\phi(x, y) = \frac{\kappa}{2\pi} \arctan \frac{y - y_0}{x - x_0}. \tag{12.3.4}$$

We recall that the velocity is the gradient of the velocity potential, $\mathbf{u} = \boldsymbol{\nabla}\phi$.
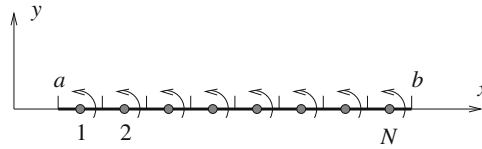
**Figure 12.3.1**   A collection of $N$ point vortices are distributed evenly along the $x$ axis inside an interval, $(a, b)$. As the number of point vortices increases, we obtain a continuous distribution yielding a vortex panel.

### 12.3.1   From point vortices to vortex panels

Consider a collection of $N$ point vortices distributed evenly along the $x$ axis inside an interval, $(a, b)$, separated by distance $\Delta x = (b - a)/N$, as illustrated in Figure 12.3.1. The $i$th point vortex is situated at the position

$$x_i = a + \tfrac{1}{2}\, i\, \Delta x, \qquad y_i = 0 \tag{12.3.5}$$

for $i = 1, \ldots, N$. The strength of the $i$th point vortex is denoted as $\kappa_i$. The first point vortex is located at $x_i = a + \frac{1}{2}\,\Delta x$ and the last point vortex is located at $x_N = b - \frac{1}{2}\,\Delta x$.

Superposing the stream functions associated with the individual point vortices, we find that the stream function of the flow induced by the collection is given by

$$\psi(x, y) = -\sum_{i=1}^{N} \frac{\kappa_i}{4\pi}\, \ln \frac{(x - x_i)^2 + (y - y_i)^2}{\varrho^2}, \tag{12.3.6}$$

which can be recast into the form

$$\psi(x, y) = -\frac{1}{4\pi}\sum_{i=1}^{N} \ln \frac{(x - x_i)^2 + (y - y_i)^2}{\varrho^2}\, \frac{\kappa_i}{\Delta x}\, \Delta x, \tag{12.3.7}$$

with the understanding that $y_i = 0$.

In the limit as $N$ tends to infinity, and correspondingly $\Delta x$ tends to zero, while the strength of the point vortices decreases so that the ratio $\gamma_i \equiv \kappa_i/\Delta x$ remains constant, the sum on the right-hand side of (12.3.7) reduces to a line integral over the domain of distribution of the point vortices, yielding the integral representation

$$\psi^{\text{vortex panel}}(x, y) = -\frac{1}{4\pi}\int_a^b \ln \frac{(x - x')^2 + (y - y')^2}{\varrho^2}\, \gamma(x')\, \mathrm{d}x', \tag{12.3.8}$$

with the understanding that $y' = 0$. The right-hand side of (12.3.8) expresses the flow due to a two-dimensional finite vortex sheet with strength density $\gamma(x)$, also called a *vortex panel*, extending between the points $x = a$ and $b$. The circulation around the panel is equal to the integral of the strength density,

$$\Gamma^{\text{vortex panel}} \equiv \int_a^b \gamma(x)\, \mathrm{d}x, \tag{12.3.9}$$

defined as the *panel strength*.

Following the discussion in Section 3.7, we find that the circulation around a closed loop that does not enclose the panel is zero, whereas the circulation around a simple loop that wraps around the panel once is equal to the panel strength. If the strength of the panel is zero, the circulation vanishes.

### 12.3.2 Vortex panels with uniform strength

It is useful to consider a vortex panel with uniform strength density, $\gamma$, equal to $\gamma^{(0)}$. According to (12.3.9), the circulation around the panel is equal to

$$\Gamma^{\text{vortex panel}} = (b - a)\,\gamma^{(0)}. \tag{12.3.10}$$

Applying (12.3.8) with $y' = 0$, we find that the stream function of the induced flow is given by

$$\psi^{(0)}(x, y) = -\frac{\gamma^{(0)}}{4\pi} \int_a^b \ln \frac{(x - x')^2 + y^2}{\varrho^2} \, dx'. \tag{12.3.11}$$

The integral on the right-hand side of (12.3.11) can be calculated with the help of standard mathematical tables, and is found to be

$$\begin{aligned}
\psi^{(0)}(x, y) = -\gamma^{(0)} \frac{1}{4\pi} \Big( &- (x - b) \ln \frac{(x - b)^2 + y^2}{\varrho^2} \\
&+ (x - a) \ln \frac{(x - a)^2 + y^2}{\varrho^2} \\
&+ 2y \Big[ \arctan \frac{y}{x - b} - \arctan \frac{y}{x - a} \Big] - 2(b - a) \Big).
\end{aligned} \tag{12.3.12}$$

The velocity components arise by straightforward differentiation, and are found to be

$$u_x^{(0)}(x, y) = \frac{\partial \psi^{(0)}}{\partial y} = -\frac{\gamma^{(0)}}{2\pi} \Big( \arctan \frac{y}{x - b} - \arctan \frac{y}{x - a} \Big) \tag{12.3.13}$$

and

$$u_y^{(0)}(x, y) = -\frac{\partial \psi^{(0)}}{\partial x} = -\frac{\gamma^{(0)}}{4\pi} \ln \frac{(x - b)^2 + y^2}{(x - a)^2 + y^2}. \tag{12.3.14}$$

The streamline pattern induced by a vortex panel subtended between the points $x = \pm b$ is shown in Figure 12.3.2. Far from the panel, the flow resembles that due to a point vortex with strength

$$\kappa = \Gamma^{\text{vortex panel}} = \gamma^{(0)}\,(b - a) = 2\,b\,\gamma^{(0)}, \tag{12.3.15}$$
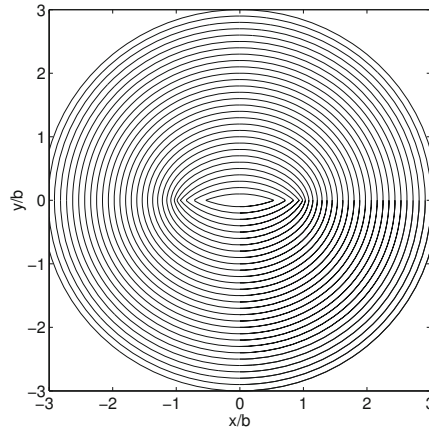
situated at the origin.

**Figure 12.3.2** Streamline pattern of the flow induced by a vortex panel with uniform strength situated along the $x$ axis in the interval $[-b, b]$.

### Jump in velocity across a vortex panel

Expression (12.3.14) shows that the $y$ component of the velocity is continuous throughout the domain of flow as well as across the vortex panel. In contrast, because of the presence of the inverse tangent function on the right-hand side of (12.3.13), the $x$ velocity component undergoes a discontinuity across the vortex panel.

To demonstrate this jump, we evaluate the velocity at a point on the upper surface of the panel for $a < x < b$ and $y = +\epsilon$, where $\epsilon$ is a small positive elevation, and find that

$$u_x^{(0)}(x, y \to 0+) = -\gamma^{(0)} \frac{1}{2\pi} \left( -\arctan(-\infty) + \arctan(+\infty) \right), \qquad (12.3.16)$$

yielding

$$u_x^{(0)}(x, y \to 0+) = -\gamma^{(0)} \frac{1}{2\pi} \left( \frac{\pi}{2} + \frac{\pi}{2} \right) \qquad (12.3.17)$$

and then

$$u_x^{(0)}(x, y \to 0_+) = -\tfrac{1}{2} \gamma^{(0)}, \qquad (12.3.18)$$

independent of $x$, provided that $a < x < b$. The $x$ velocity component at a point at the lower surface of the panel for $a < x < b$ and $y = -\epsilon$ is given by

$$u_x^{(0)}(x, \to 0_-) = -\gamma^{(0)} \frac{1}{2\pi} \left( -\arctan(+\infty) + \arctan(-\infty) \right), \qquad (12.3.19)$$

yielding

$$u_x^{(0)}(x, \to 0_-) = -\gamma^{(0)} \frac{1}{2\pi} \left( -\frac{\pi}{2} - \frac{\pi}{2} \right), \qquad (12.3.20)$$

and then

$$u_x^{(0)}(x, \to 0_-) = \tfrac{1}{2}\,\gamma^{(0)}, \tag{12.3.21}$$

independent of $x$, provided that $a < x < b$.

Using the preceding results, we find that, as the vortex panel is traversed from the upper to the lower side, the velocity undergoes a discontinuity whose magnitude is equal to the strength of the vortex sheet,

$$u_x(x, -\epsilon) - u_x(x, +\epsilon) = \gamma^{(0)}. \tag{12.3.22}$$

In contrast, a discontinuity does not occur beyond the edges of the vortex panel.

These observations suggest that a vortex panel, or more generally a vortex sheet, can be identified with a surface across which the tangential component of the velocity undergoes a discontinuity, where the magnitude of the discontinuity is the strength of the vortex panel or vortex sheet.

### 12.3.3  *Vortex panel with linear strength density*

Next, we consider a vortex panel situated in the interval $[a, b]$ along the $x$ axis, with linear strength density distribution given by

$$\gamma(x) = \gamma^{(0)} + \gamma^{(1)}\,(x - a). \tag{12.3.23}$$

Using (12.3.9), we find that the circulation around the panel is

$$\Gamma^{\text{vortex panel}} = \int_a^b \gamma\,\mathrm{d}x = (b-a)\left[\,\gamma^{(0)} + \tfrac{1}{2}\gamma^{(1)}(b-a)\,\right] \tag{12.3.24}$$

or

$$\Gamma^{\text{vortex panel}} = (b-a)\,\gamma(\frac{a+b}{2}). \tag{12.3.25}$$

Applying (12.3.8) with $y' = 0$ and rearranging, we find that the stream function of the induced flow is given by

$$\psi^{(01)}(x, y) = -\frac{\gamma^{(0)} + \gamma^{(1)}(x-a)}{4\pi} \int_a^b \ln \frac{(x-x')^2 + y^2}{\varrho^2}\,\mathrm{d}x'$$
$$-\frac{\gamma^{(1)}}{4\pi} \int_a^b (x'-x)\,\ln \frac{(x-x')^2 + y^2}{\varrho^2}\,\mathrm{d}x'. \tag{12.3.26}$$

The first integral on the right-hand side of (12.3.26) is equal to the expression enclosed by the tall parentheses following the fraction on the right-hand side of (12.3.12). The second

integral can be calculated with the help of standard tables of integrals and is found to be

$$\int_a^b (x' - x) \ln \frac{(x - x')^2 + y^2}{\varrho^2} \, \mathrm{d}x' = \tfrac{1}{2} \left[ (x - b)^2 + y^2 \right] \ln \frac{(x - b)^2 + y^2}{\varrho^2}$$

$$- \tfrac{1}{2} \left[ (x - a)^2 + y^2 \right] \ln \frac{(x - a)^2 + y^2}{\varrho^2} - \tfrac{1}{2}(x - b)^2 + \tfrac{1}{2}(x - a)^2. \tag{12.3.27}$$

Combining (12.3.11), (12.3.27), and (12.3.8), and consolidating various terms, we obtain

$$\psi^{(01)}(x, y) = \psi^{(0)}(x, y) + \psi^{(1)}(x, y), \tag{12.3.28}$$

where $\psi^{(0)}$ is given in (12.3.12) and

$$\psi^{(1)}(x, y) = -\gamma^{(1)} \frac{1}{4\pi} \left( \tfrac{1}{2} \left[ y^2 - (x - b)(x + b - 2a) \right] \ln \frac{(x - b)^2 + y^2}{\varrho^2} \right.$$

$$- \tfrac{1}{2} \left[ y^2 - (x - a)^2 \right] \ln \frac{(x - a)^2 + y^2}{\varrho^2} + 2y (x - a) \left( \arctan \frac{y}{x - b} - \arctan \frac{y}{x - a} \right)$$

$$\left. - \frac{1}{2}(x - b)^2 + \frac{1}{2}(x - a)^2 - 2(x - a)(b - a) \right). \tag{12.3.29}$$

The velocity components can be resolved into corresponding constituents,

$$u_x^{(01)}(x, y) = u_x^{(0)}(x, y) + u_x^{(1)}(x, y) \tag{12.3.30}$$

and

$$u_y^{(01)}(x, y) = u_y^{(0)}(x, y) + u_y^{(1)}(x, y), \tag{12.3.31}$$

where $u_x^{(0)}$ and $u_y^{(0)}$ are given in (12.3.13) and (12.3.14). Tedious differentiation yields the final forms

$$u_x^{(1)}(x, y) = \frac{\partial \psi^{(1)}}{\partial y} = -\gamma^{(1)} \frac{1}{4\pi} \left( y \ln \frac{(x - b)^2 + y^2}{(x - a)^2 + y^2} \right.$$

$$\left. + 2(x - a) \left( \arctan \frac{y}{x - b} - \arctan \frac{y}{x - a} \right) \right) \tag{12.3.32}$$

and

$$u_y^{(1)}(x, y) = -\frac{\partial \psi^{(1)}}{\partial x} = -\gamma^{(1)} \frac{1}{4\pi} \left( (x - a) \ln \frac{(x - b)^2 + y^2}{(x - a)^2 + y^2} \right.$$

$$\left. - 2y \left( \arctan \frac{y}{x - b} - \arctan \frac{y}{x - a} \right) + 2(b - a) \right). \tag{12.3.33}$$

Using these expressions, we confirm that, as the vortex panel is traversed along the $y$ axis from the upper to the lower side, the $x$ velocity component undergoes a discontinuity whose magnitude is equal to the local strength of the vortex sheet.
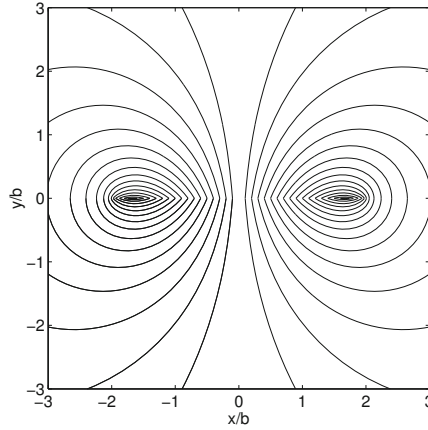
**Figure 12.3.3**  Streamline pattern of the flow due to a vortex panel with linear strength situation along the $x$ axis in the interval $[-b, b]$, for vanishing circulation around the panel.

The streamline pattern of the flow induced by a vortex panel extending in the interval $[-b, b]$ is shown in Figure 12.3.3 for $\gamma^{(1)} = -\gamma^{(0)}/b$, so that $\gamma(x) = \gamma^{(0)} x/b$. Because the circulation around the panel vanishes, as required by (12.3.25), far from the panel, the flow reduces to that due to a point-vortex dipole situated at the panel center-point and oriented along the $x$ axis. Alternatively, the far flow is identical to the flow due to a point-source dipole placed at the same location oriented along the $y$ axis.

### PROBLEM

**12.3.1** *Velocity potential due to vortex panels.*

(*a*) Confirm that the velocity potential corresponding to the stream function stated in (12.3.12) is given by

$$\phi^{(0)}(x, y) = -\gamma^{(0)} \frac{1}{2\pi} \Big( (x - b) \arctan \frac{y}{x - b} - (x - a) \arctan \frac{y}{x - a}$$
$$+ \tfrac{1}{2} y \ln \frac{(x - b)^2 + y^2}{(x - a)^2 + y^2} \Big). \qquad (12.3.34)$$

(*b*) Confirm that the velocity potential corresponding to the stream function given in (12.3.29) is given by

$$\phi^{(1)}(x, y) = -\gamma^{(1)} \frac{1}{4\pi} \Big( (x - a) y \ln \frac{(x - b)^2 + y^2}{(x - a)^2 + y^2}$$
$$+ \big[ (x - a)^2 - (b - a)^2 - y^2 \big] \arctan \frac{y}{x - b} \qquad (12.3.35)$$
$$- \big[ (x - a)^2 - y^2 \big] \arctan \frac{y}{x - a} + y(b - a) \Big).$$
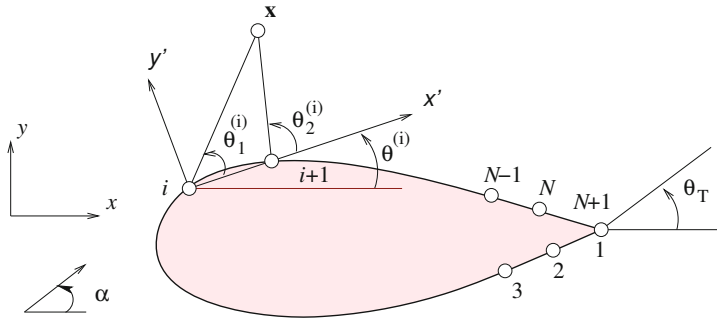
**Figure 12.4.1** Discretization of the contour of an airfoil into $N$ flat panels defined by a set of $N+1$ nodes.

## 12.4 Vortex panel method

In Section 12.3, we introduced vortex panels with constant or linear density distributions and studied the properties of the induced flows. In this section, we employ these flows as elementary units into a vortex-panel method that allows us to compute an irrotational flow past a two-dimensional airfoil with the Kutta–Joukowski condition satisfied at the trailing edge.

The key idea is to express a flow of interest as a superposition of ($a$) an incident streaming flow and ($b$) a collection of flows induced by vortex panels with *a priori* unknown strength densities distributed around an airfoil. The panel strength densities are then computed to satisfy the no-penetration boundary condition around the airfoil.

### Contour discretization

Shown in Figure 12.4.1 is a schematic illustration of uniform (streaming) flow with velocity $\mathbf{U} = (U_x, U_y)$ past an airfoil for angle of attack $\alpha$. In the first strep of the vortex panel method, the contour of the airfoil is traced with $N + 1$ nodes distributed in the clockwise direction, where points labeled 1 and $N + 1$ coincide with the trailing edge.

A pair of successive nodes, $\mathbf{x}^{(i)}$ and $\mathbf{x}^{(i+1)}$, defines a flat vortex panel labeled $i$ for $i = 1, \ldots, N$. The union of the $N$ vortex panels defines a polygonal contour which is an approximation to the generally curved contour of the airfoil.

### Flow representation

In the vortex-panel method, the velocity at a field point, $\mathbf{x} = (x, y)$, is expressed by the

superposition

$$\mathbf{u}(x,y) = \mathbf{U} + \sum_{i=1}^{N} \mathbf{u}^{(i)}(x,y), \tag{12.4.1}$$

where $\mathbf{u}^{(i)}(x,y)$ is the velocity induced by the $i$th vortex panel.

In the implementation discussed in this section, panels with linear strength density are employed. The strength density of the $i$th panel varies linearly from the value $\gamma_i$ assigned to the $i$th node, which is the first point of the $i$th panel, to the value $\gamma_{i+1}$ assigned to the $i+1$ node, which is the second point of the $i$th panel. The $N+1$ unknown values, $\gamma_i$ for $i = 1, \ldots, N+1$, must be computed to satisfy the no-penetration condition around the airfoil in some approximate sense.

A key observation that the velocity induced by the $i$th panel, $\mathbf{u}^{(i)}(x,y)$, is determined by the position and strength density of the panel at the two end points. To signify this dependence, we write

$$\mathbf{u}^{(i)}(x,y) = \mathbf{u}^{\text{LVP}}(x,y\,;\,\mathbf{x}^{(i)},\mathbf{x}^{(i+1)},\gamma^{(i)},\gamma^{(i+1)}). \tag{12.4.2}$$

where LVP stands for *linear vortex panel.* Next, we proceed to develop a method for computing the velocity induced by the individual panels.

### *Panel-induced velocity in global coordinates*

It is helpful to introduce a local coordinate system, $(x',y')$, where the $x'$ axis passes through the two end points of the $i$th panel, $\mathbf{x}^{(i)}$ and $\mathbf{x}^{(i+1)}$, and set the origin at the first end point $\mathbf{x}^{(i)}$, as shown in Figure 12.4.1. The coordinates of a point in the local system, $(x',y')$, are related to those in the global system, $(x,y)$, by the equations

$$\begin{aligned}
x' &= \phantom{-}(x - x^{(i)})\cos\theta^{(i)} + (y - y^{(i)})\sin\theta^{(i)}, \\
y' &= -(x - x^{(i)})\sin\theta^{(i)} + (y - y^{(i)})\cos\theta^{(i)},
\end{aligned} \tag{12.4.3}$$

where $\theta^{(i)}$ is the inclination of the $i$th panel defined in Figure 12.4.1.

Next, we express the strength density of the $i$th panel in the linear form

$$\gamma(x') = \gamma^{(0)} + \gamma^{(1)}(x' - x'^{(i)}), \tag{12.4.4}$$

with the understanding that $x'^{(i)} = 0$, and require that

$$\begin{aligned}
\gamma\big(x' = x'^{(i)}\big) &= \gamma^{(0)} = \gamma^{(i)}, \\
\gamma\big(x' = x'^{(i+1)}\big) &= \gamma^{(0)} + \gamma^{(1)}(x'^{(i+1)} - x'^{(i)}) = \gamma^{(i+1)},
\end{aligned} \tag{12.4.5}$$

to find that

$$\gamma^{(0)} = \gamma^{(i)}, \qquad \gamma^{(1)} = \frac{\gamma^{(i+1)} - \gamma^{(i)}}{\Delta\ell_i}, \tag{12.4.6}$$

where

$$\Delta \ell_i = \left( (x^{(i+1)} - x^{(i)})^2 + (y^{(i+1)} - y^{(i)})^2 \right)^{1/2} = x'^{(i+1)} - x'^{(i)} \qquad (12.4.7)$$

is the length of the $i$th panel computed in terms of the global (unprimed) or local (primed) coordinates of the two panel end-points.

Reviewing the results of Section 12.3, we find that the $x'$ and $y'$ components of the velocity induced by the $i$th panel are given by equations (12.3.30) and (12.3.31), subject to the following substitutions:

$$
\begin{array}{ccc}
a & \rightarrow & 0 \\
b & \rightarrow & x'^{(i+1)} \\
\gamma^{(0)} & \rightarrow & \gamma^{(i)} \\
\gamma^{(1)} & \rightarrow & (\gamma^{(i+1)} - \gamma^{(i)})/\Delta \ell_i \\
x & \rightarrow & x' \\
y & \rightarrow & y'
\end{array}
\qquad (12.4.8)
$$

After carrying out some algebra, we find that the velocity components of the flow induced by the $i$th panel in the local frame are given by

$$u_{x'}^{(i)}(x', y') = a_{x'}^{(i,1)} \gamma^{(i)} + a_{x'}^{(i,2)} \gamma^{(i+1)}, \qquad (12.4.9)$$

and

$$u_{y'}^{(i)}(x', y') = a_{y'}^{(i,1)} \gamma^{(i)} + a_{y'}^{(i,2)} \gamma^{(i+1)}, \qquad (12.4.10)$$

where $a_{x'}^{(i,1)}, a_{x'}^{(i,2)}, a_{y'}^{(i,1)}$, and $a_{y'}^{(i,2)}$ are *local influence coefficients* given by

$$a_{x'}^{(i,1)} = \frac{1}{2\pi x_2'} \left( y' c + (x' - x_2') \Delta \theta' \right),$$

$$a_{y'}^{(i,1)} = \frac{1}{2\pi x_2'} \left( (x' - x_2') c - y' \Delta \theta' + x_2' \right),$$

$$a_{x'}^{(i,2)} = -\frac{1}{2\pi x_2'} \left( y' c + x' \Delta \theta' \right), \qquad (12.4.11)$$

$$a_{y'}^{(i,2)} = -\frac{1}{2\pi x_2'} \left( x' c - y' \Delta \theta' + x_2' \right),$$

subject to the following definitions:

$$x_2' \equiv x'^{(i+1)}, \qquad \Delta \theta' \equiv \theta_2' - \theta_1', \qquad \theta_2' \equiv \arctan \frac{y'}{x' - x_2'},$$

$$\theta_1' \equiv \arctan \frac{y'}{x'}, \qquad c \equiv \log \left( \frac{(x' - x_2')^2 + y'^2}{x'^2 + y'^2} \right)^{1/2}. \qquad (12.4.12)$$

To recover the velocity components in the global frame, we use the inverse of the coordinate transformation shown in (12.4.3),

$$u_x^{(i)}(x,y) = u_{x'}^{(i)}(x',y') \cos\theta^{(i)} - u_{y'}^{(i)}(x',y') \sin\theta^{(i)} \qquad (12.4.13)$$

and

$$u_y^{(i)}(x,y) = u_{x'}^{(i)}(x',y') \sin\theta^{(i)} + u_{y'}^{(i)}(x',y') \cos\theta^{(i)}. \qquad (12.4.14)$$

Substituting expressions (12.4.9) and (12.4.10) into the right-hand sides of equations (12.4.13) and (12.4.14), and rearranging, we derive explicit relations in terms of the strength of the vortex panel at the end points,

$$\begin{aligned} u_x^{(i)}(x,y) &= a_x^{(i,1)}\gamma^{(i)} + a_x^{(i,2)}\gamma^{(i+1)}, \\ u_y^{(i)}(x,y) &= a_y^{(i,1)}\gamma^{(i)} + a_{y'}^{(i,2)}\gamma^{(i+1)}, \end{aligned} \qquad (12.4.15)$$

where $a_x^{(i,1)}, a_x^{(i,2)}, a_y^{(i,1)}$, and $a_y^{(i,2)}$ are *global influence coefficients* given by

$$\begin{aligned} a_x^{(i,1)}(x,y) &= a_{x'}^{(i,1)}(x',y') \cos\theta^{(i)} - a_{y'}^{(i,1)}(x',y') \sin\theta^{(i)}, \\ a_x^{(i,2)}(x,y) &= a_{x'}^{(i,2)}(x',y') \cos\theta^{(i)} - a_{y'}^{(i,2)}(x',y') \sin\theta^{(i)}, \\ a_y^{(i,1)}(x,y) &= a_{x'}^{(i,1)}(x',y') \sin\theta^{(i)} + a_{y'}^{(i,1)}(x',y') \cos\theta^{(i)}, \\ a_y^{(i,2)}(x,y) &= a_{x'}^{(i,2)}(x',y') \sin\theta^{(i)} + a_{y'}^{(i,2)}(x',y') \cos\theta^{(i)}. \end{aligned} \qquad (12.4.16)$$

Given the coordinates of the evaluation point, $(x,y)$, we may evaluate these coefficients by carrying out the following steps:

1. Compute the panel inclination angle, $\theta^{(i)}$, and the panel length from the expressions given in (12.4.6) and (12.4.7).

2. Compute the local coordinates $(x',y')$ using (12.4.3).

3. Compute the local influence coefficients using (12.4.11).

4. Compute the global influence coefficients using (12.4.16).

The procedure is readily implemented in a computer code.

### 12.4.1   *Velocity in terms of the panel strength*

Substituting expressions (12.4.15) into the right-hand side of (12.4.1), we obtain explicit expressions for the global components of the velocity in terms of the strength of the vortex panels at the end-nodes,

$$\begin{aligned} u_x(x,y) &= U_x + \sum_{i=1}^{N} \left( a_x^{(i,1)}(x,y)\,\gamma^{(i)} + a_x^{(i,2)}(x,y)\,\gamma^{(i+1)} \right), \\ u_y(x,y) &= U_y + \sum_{i=1}^{N} \left( a_y^{(i,1)}(x,y)\,\gamma^{(i)} + a_y^{(i,2)}(x,y)\,\gamma^{(i+1)} \right). \end{aligned} \qquad (12.4.17)$$

For convenience, we write

$$
\begin{aligned}
u_x(x,y) &= U_x + \sum_{i=1}^{N+1} b_x^{(i)}(x,y)\,\gamma^{(i)}, \\
u_y(x,y) &= U_y + \sum_{i=1}^{N+1} b_y^{(i)}(x,y)\,\gamma^{(i)},
\end{aligned}
\tag{12.4.18}
$$

where

$$
\begin{aligned}
b_w^{(1)}(x,y) &= a_w^{(1,1)}(x,y), \\[4pt]
b_w^{(2)}(x,y) &= a_w^{(1,2)}(x,y) + a_w^{(2,1)}(x,y), \\[4pt]
b_w^{(3)}(x,y) &= a_w^{(2,2)}(x,y) + a_w^{(3,1)}(x,y), \\
&\cdots, \\
b_w^{(N)}(x,y) &= a_w^{(N-1,2)}(x,y) + a_w^{(N,1)}(x,y), \\[4pt]
b_w^{(N+1)}(x,y) &= a_w^{(N,2)}(x,y)
\end{aligned}
\tag{12.4.19}
$$

for $w = x, y$ is a new set of influence coefficients.

### **12.4.2 Point collocation**

If we knew the strength of the vortex panels at the nodes, we would be able to use equations (12.4.18) to evaluate the velocity at any point in the flow. The fundamental idea underlying the vortex-panel method is that the $N+1$ unknown values, $\gamma^{(i)}$ for $i = 1, \ldots, N+1$, should be computed to satisfy the no-penetration condition at a point **x** located around the airfoil contour,

$$
\mathbf{u}(\mathbf{x}) \cdot \mathbf{n}(\mathbf{x}) = 0,
\tag{12.4.20}
$$

where **n** is the unit vector normal to the airfoil.

In the panel-collocation method, $N$ equations emerge by requiring that (12.4.20) is satisfied at the mid-point of each panel located at

$$
\mathbf{x}_{\mathrm{M}}^{(j)} = \tfrac{1}{2}\left(\mathbf{x}^{(j)} + \mathbf{x}^{(j+1)}\right)
\tag{12.4.21}
$$

for $j = 1, \ldots, N$. Using (12.4.18) to express the velocity in terms of the strength of the vortex sheet and rearranging, we obtain

$$
\sum_{i=1}^{N+1} A_{i,j}\,\gamma^{(i)} = -U_x\,n_x(x_{\mathrm{M}}^{(j)}, y_{\mathrm{M}}^{(j)}) - U_y\,n_y(x_{\mathrm{M}}^{(j)}, y_{M}^{(j)}),
\tag{12.4.22}
$$

where

$$A_{i,j} \equiv b_x^{(i)}\big(x_{\mathrm{M}}^{(j)}, y_{\mathrm{M}}^{(j)}\big)\, n_x(x_M^{(j)}, y_M^{(j)}) + b_y^{(i)}\big(x_{\mathrm{M}}^{(j)}, y_{\mathrm{M}}^{(j)}\big)\, n_y(x_M^{(j)}, y_M^{(j)}). \qquad (12.4.23)$$

It is important to bear in mind that, when $i = j$, the self-induced velocity is evaluated at the mid-point of the panel on the side of the flow exterior to the airfoil. With reference to equations (12.4.11), this means that $y' = 0$, $c = 0$, and $\Delta\theta' = \pi$. Applying equation (12.4.22) for $j = 1, \ldots, N$, we obtain a system of $N$ linear algebraic equations for the $N + 1$ unknowns, $\gamma^{(i)}$.

### Kutta–Joukowski condition

One degree of freedom is available and can be used to arbitrarily specify the circulation around the airfoil. In Section 12.4.2, we saw that, in practice, the circulation established around the airfoil is such that the Kutta–Joukowski condition is fulfilled at the trailing edge.

In our formulation, the Kutta–Joukowski condition is implemented by requiring that the strength of the vortex sheet on the upper side of the airfoil at the trailing edge is equal in magnitude and opposite in sign to the strength of the vortex sheet on the lower side of the airfoil at the trailing edge. The mathematical statement of the Kutta–Joukowski condition is then

$$\gamma^{(1)} = -\gamma^{(N+1)}. \qquad (12.4.24)$$

Appending this equation to equation (12.4.22) written for $j = 1, \ldots, N$, we obtain the desired system of $N + 1$ equations for the $N + 1$ unknowns, $\gamma^{(i)}$. The solution can be computed using, for example, the method of Gauss elimination discussed in Section 3.4.

### 12.4.3   Circulation and pressure coefficient

Once the strength of the vortex sheet is available, the tangential velocity, $u_t = \mathbf{u} \cdot \mathbf{t}$, can be evaluated from the discrete representation (12.4.18), where $\mathbf{t}$ is the unit vector tangent to the airfoil pointing along the local $x'$ axis.

The circulation around the airfoil can be approximated either with the expression

$$C = -\sum_{i=1}^{N} u_t(\mathbf{x}_{\mathrm{M}}^{(i)})\, \Delta\ell_i \qquad (12.4.25)$$

or with the expression

$$C = \tfrac{1}{2}\sum_{i=1}^{N}(\gamma^{(i)} + \gamma^{(i+1)})\, \Delta\ell_i, \qquad (12.4.26)$$

where $\Delta\ell_i$ is the length of the $i$th panel. The second expression implements the trapezoidal rule for integrating the strength of the vortex sheet with respect to arc length, $\ell$, around the airfoil.

The dimensionless pressure coefficient at the panel mid-points is defined by the expression

$$c_p^{(i)} \equiv \frac{p(\mathbf{x}_M^{(i)}) - p_\infty}{\frac{1}{2} \rho U^2} = 1 - \frac{u_t^2(\mathbf{x}_M^{(i)})}{U^2}, \tag{12.4.27}$$

where $p_\infty$ is the pressure at infinity and

$$U^2 \equiv U_x^2 + U_y^2 \tag{12.4.28}$$

is the square of the magnitude of the velocity of the incident streaming flow.

The streamline pattern, distribution of panel strength, and distribution of the pressure coefficient around a NACA airfoil computed by the code *airf_2d_lvp* discussed in Section 12.4.5 is shown in Figure 12.4.2. The results confirm that high pressure occurs at the lower surface of the airfoil and low pressure occurs at the upper surface of the airfoil; the difference generates a lift force.

### 12.4.4 Lift

In the absence of viscous stresses, the force exerted on the airfoil is given by the pressure integral

$$\mathbf{F} = \oint (-p)\, \mathbf{n}\, d\ell = -\frac{1}{2}\, \rho U^2 \oint \left( c_p + \frac{p^\infty}{\frac{1}{2}\rho U^2} \right) \mathbf{n}\, d\ell, \tag{12.4.29}$$

where $\mathbf{n}$ is the unit vector normal to the airfoil pointing into the fluid, and $\ell$ is the arc length around the airfoil. Since the integral of the normal vector around a closed contour is identically zero,

$$\mathbf{F} = -\frac{1}{2}\, \rho U^2 \oint c_p\, \mathbf{n}\, d\ell, \tag{12.4.30}$$

Using the mid-point rule to approximate the two scalar components of the vector integral in (12.4.30), we obtain the following expressions for the dimensionless $x$ and $y$ force components,

$$\widehat{F}_x \equiv \frac{F_x}{\frac{1}{2}\rho U^2} = -\sum_{i=1}^{N} c_p^{(i)}\, n_x^{(i)}\, \Delta\ell_i \tag{12.4.31}$$

and

$$\widehat{F}_y \equiv \frac{F_y}{\frac{1}{2}\rho U^2} = -\sum_{i=1}^{N} c_p^{(i)}\, n_y^{(i)}\, \Delta\ell_i. \tag{12.4.32}$$

The scaled lift force with respect to the wind axis is defined as the component of the force normal to the direction of the incident flow, given by

$$\widehat{L}_w = \widehat{F}_y \cos\alpha - \widehat{F}_x \sin\alpha, \tag{12.4.33}$$

(*a*)
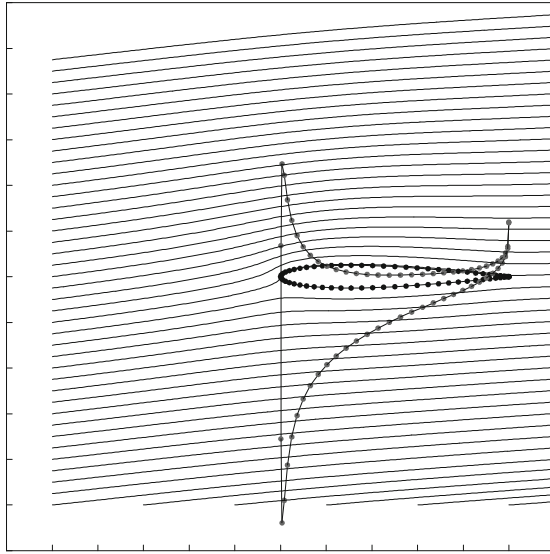


(*b*)
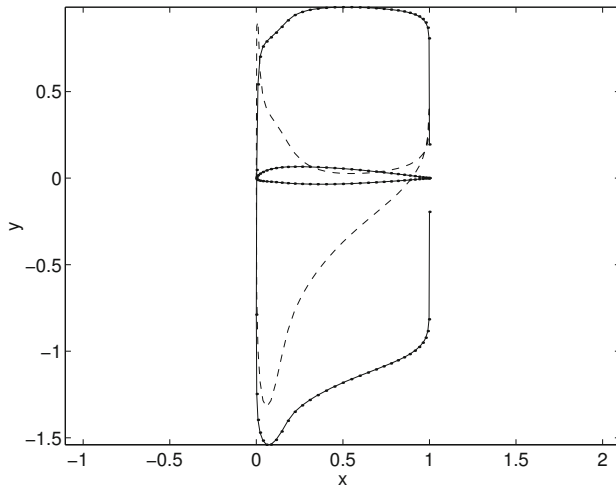


**Figure 12.4.2**   (*a*) Streamline pattern and distribution of the pressure coefficient on the upper and lower surfaces of an airfoil for angle of attack $\alpha = 5°$, computed using the linear vortex panel method. (*b*) Distribution of the pressure coefficient (dashed line) and panel strength (connected dots) around another airfoil. These solutions were generated by the FDLIB code *airf_2d_lvp*.

where $\alpha$ is the angle of attack, as shown in Figure 12.4.1. According to the Kutta–Joukowski theorem expressed by equation (12.2.4),

$$\widehat{L}_w = -2\frac{C}{U}. \tag{12.4.34}$$

The difference in the values of the lift predicted by (12.4.33) or (12.4.34) is a measure of the accuracy of the numerical method.

### 12.4.5 Vortex panel code

The following MATLAB code entitled *airf_2d_lvp,* located in directory *07_ptf* of FDLIB, implements the linear vortex panel method:

```
%===========================
% linear vortex panel method
%===========================

Npl = 64;    % number of panels
chord = 1.0;   % chord
thick = 0.1;   % airfoil thickness
Umag = 1.0;   % incident velocity
alpha = 4.0;   % angle of attack in degrees

%----
% generate the NACA 23012 airfoil contour
% ep are the panel end points
%----

ep = naca(chord,thick,Npl);

%---
% coordinates of the panel end points
%---

for i=1:Npl
  pt1(i,1) = ep(i,1);
  pt1(i,2) = ep(i,2);
  pt2(i,1) = ep(i+1,1);
  pt2(i,2) = ep(i+1,2);
end

%-------------------------------------
% compute:
%
% 1.   panel inclination angle th(j) between -pi and pi
% 2.   panel lengths
% 3.   tangential and normal unit vectors
%-------------------------------------
```

```
for i=1:Npl
  dx = pt2(i,1)-pt1(i,1);
  dy = pt2(i,2)-pt1(i,2);
  dl(i) = sqrt( (pt2(i,1)-pt1(i,1))^2 ...    % panel length
      + (pt2(i,2)-pt1(i,2))^2);
  th(i) = atan2(dy,dx);
  tnx(i) = cos(th(i));   % tangential vector
  tny(i) = sin(th(i));
  vnx(i) = -tny(i);   % normal vector points into flow
  vny(i) = tnx(i);
end

%---
% collocation points are panel mid-points
%---

for i=1:Npl
  co(i,1) = 0.5*(pt1(i,1)+pt2(i,1));
  co(i,2) = 0.5*(pt1(i,2)+pt2(i,2));
end

%-------------------------------------
% compute the influence coefficients
% and right-hand side of linear system
%-------------------------------------

for i=1:Npl   % OVER COLLOCATION POINTS; ENDS AT THE RABBIT

%---
% compute influence of jth panel
% on ith collocation point
%---

for j=1:Npl   % OVER PANELS; ENDS AT THE DOG

%---
% Compute the local panel coordinates (x, y)
% The first panel point is located at the shifted origin;
% the panel becomes horizontal
%---

xt = co(i,1) - pt1(j,1);   % shift collocation point
yt = co(i,2) - pt1(j,2);
x = xt*tnx(j) + yt*tny(j);   % and rotate
y = -xt*tny(j) + yt*tnx(j);
x1 = 0.0; y1 = 0.0;
x2t = pt2(j,1) - pt1(j,1);   % shift second-end point
y2t = pt2(j,2) - pt1(j,2);
```

```
x2 = x2t*tnx(j) + y2t*tny(j);    % and rotate y2 = 0.0;


%---
% Compute radial distances:  r1, r2
% subtended angles:  th1, th2
%---

r1 = sqrt(x*x+y*y);
r2 = sqrt((x-x2)*(x-x2)+y*y);
th1 = atan2(y,x);
th2 = atan2(y,x-x2);


%-------------------------------------------
% gamma1, gamma2 are the vortex sheet strengths
% at the first and second panel points.
%
% Compute influence coefficients associated with
% the velocity components (ux, uy)
% corresponding to gamma1 and gamma, so that:
%
% ux = ax1*gamma1 + ax2*gamma2
% uy = ay1*gamma1 + ay2*gamma2
%
% These velocities are in
% the jth-panel reference frame.
%-------------------------------------------

if(i==j)    % self-induced velocity
  ax1 = 0.5*(x/x2-1.0);
  ay1 = 1.0/(2*pi);
  ax2 =-0.5*x/x2;
  ay2 =-1.0/(2*pi);
else
  dth = th2-th1;
  rrt = r2/r1;
  rrtl = log(rrt);
  fcc = 1.0/(2*pi*x2);
  ax1 = fcc*( y*rrtl + (x-x2)*dth );
  ay1 = fcc*((x-x2)*rrtl - y*dth + x2);
  ax2 = -fcc*(y*rrtl + x*dth );
  ay2 = -fcc*(x*rrtl - y*dth + x2);
end


%---
% transform the influence coefficient into the
% global reference frame by rotation
%---

ux1 = ax1*tnx(j) - ay1*tny(j);
```

```
uy1 = ax1*tny(j) + ay1*tnx(j);
ux2 = ax2*tnx(j) - ay2*tny(j);
uy2 = ax2*tny(j) + ay2*tnx(j);

%------------------------------------------------
% Compute the coefficients of gamma in the
% master influence matrix.
%
% These are the velocity influence coefficients
% projected onto the normal vector of ith panel
%------------------------------------------------

if(j==1)
  a(i,1)= ux1*vnx(i) + uy1*vny(i);
  holda = ux2*vnx(i) + uy2*vny(i);    % hold for the next panel
elseif(j==Npl)
  a(i,Npl) = ux1*vnx(i) + uy1*vny(i) + holda;
  a(i,Npl+1) = ux2*vnx(i) + uy2*vny(i);
else
  a(i,j)= ux1*vnx(i) + uy1*vny(i) + holda;
  holda = ux2*vnx(i) + uy2*vny(i);    % hold for the next panel
end

%--------------------------------------------------------
% b are tangential velocity influence coefficients
%
% These are the velocity influence coefficients
% projected onto the tangential vector of the ith panel
%--------------------------------------------------------

if(j==1)
  b(i,1)= ux1*tnx(i) + uy1*tny(i);
  holdb = ux2*tnx(i) + uy2*tny(i);    % hold for the next panel
elseif(j==Npl)
  b(i,Npl) = ux1*tnx(i) + uy1*tny(i) + holdb;
  b(i,Npl+1) = ux2*tnx(i) + uy2*tny(i);
else
  b(i,j)= ux1*tnx(i) + uy1*tny(i) + holdb;
  holdb = ux2*tnx(i) + uy2*tny(i);    % hold for the next panel
end

end % OVER PANELS - DOG

end % OVER COLLOCATION POINTS - RABBIT

%--------------------------------
% Add the Kutta condition
% expressed by the Npl+1 equation:
%
```

```
% The strength of the sheet at the first point
% of the first panel is equal and opposite
% to the strength of the sheet at the last point
% of the last panel,
% so that the mean value vanishes
%-----------------------------

a(Npl+1,1) = 1.0;
a(Npl+1,Npl+1) = 1.0;

%--------------------
% set right-hand side
%--------------------

al = alpha*pi/180.0;
cal = cos(al); sal = sin(al);
Ux = Umag*cal; Uy = Umag*sal;

for i=1:Npl
  rhs(i) = -Ux*vnx(i)-Uy*vny(i);
end

rhs(Npl+1)=0.0;

%-----------------------
% solve the linear system
%-----------------------

gamma = rhs/a';

%-------------------------------
% compute c_p and the circulation
%-------------------------------

circul = 0.0;    % circulation
circulg = 0.0;   % circulation in terms of gamma

for i=1:Npl
  velt = Ux*tnx(i)+Uy*tny(i); % tangential velocity
  for j=1:Npl+1
    velt = velt + b(i,j)*gamma(j);
  end
  circul = circul - velt*dl(i);    % circulation
  circulg = circulg ...
    +0.5*(gamma(i)+gamma(i+1))*dl(i);   % circulation
  cp(i) = 1.0-velt*velt/(Umag*Umag);   % press coeff
end

cp(Npl+1)=cp(1);
```

```
%---
% plotting
%---

patch(ep(:,1),ep(:,2),'y')
plot(ep(:,1),ep(:,2),'k.-')
plot(ep(:,1),cp,'--')
plot(ep(:,1),gamma,'r:')
xlabel('x','fontsize',15)
ylabel('y','fontsize',15)
```

The airfoil profile is generated by the following MATLAB function entitled *naca*, located in directory *07_ptf* of FDLIB:

```
function [ep] = naca(chord,thick,Npl)

%----
% generate the NACA 23012 airfoil contour
% ep are the panel end-points
%----

dpsi = 2*pi/Npl;

ep(1,1) = chord;
ep(1,2) = 0.0;

for i=2:Npl

  psi = (i-1.0)*dpsi;
  x = 0.5*(1.0+cos(psi));

%---
% camber line:
%---

  if(x<0.2025)
    yc = 2.6595*x*(0.1147+x*(-0.6075+x));
  else
    yc = 0.02208*(1.0-x);
  end

%---
% thickness:
%---

  yt = 5.0*thick*(0.2969*sqrt(x) ...
    -0.1260*x -0.3516*x*x +0.2843*x*x*x ...
    -0.1036*x*x*x*x );
```

```
    if(i<=(Npl/2+1))
       y = yc-yt;
    else
       y = yc+yt;
    end

    ep(i,1) = x*chord;
    ep(i,2) = y*chord;
  end

  ep(Npl+1,1) = chord;   % trailing edge
  ep(Npl+1,2) = 0.0;     % trailing edge

  %---
  % done
  %---

  return
```

The graphics display generated by the code is shown in Figure 12.4.2(*b*). The dots connected by a line describes the distribution of the panel strength, and the dashed line describes the distribution of the pressure coefficient.

**PROBLEM**

**12.4.1** ▣ *Linear vortex panel method*

(*a*) Run the code *airf_2d_lvp* for an airfoil shape of your choice. Prepare graphs and discuss the distribution of the panel strength and pressure coefficient.

(*b*) Evaluate the velocity at several points inside the airfoil and discuss the results.

## 12.5   Vortex sheet representation

Consider the vortex panel method for flow past a two-dimensional airfoil discussed in Section 12.4. In the limit as the number of panels, $N$, tends to infinity, the piecewise linear strength distributions over the individual panels describe a smooth distribution defined around the airfoil contour. Correspondingly, the sum on the right-hand side of equation (12.4.1) reduces to an integral with respect to arc length around the airfoil contour, representing the velocity induced by a vortex sheet with a generally curved shape.

Generalizing expression (12.3.8), we find that the stream function associated with the vortex sheet is given by

$$\psi^{\text{vortex sheet}}(x, y) = -\frac{1}{4\pi} \oint \ln \frac{(x - x')^2 + (y - y')^2}{\varrho^2} \, \gamma(x') \, \mathrm{d}\ell', \qquad (12.5.1)$$

where $\mathrm{d}\ell' = (\,\mathrm{d}x'^2 + \mathrm{d}y'^2\,)^{1/2}$ is the differential arc length around the airfoil measured in the

clockwise direction starting at the trailing edge, and the integration is performed around the airfoil contour.

Conversely, the vortex-panel representation can be regarded as the result of discretizing the integral on the right-hand side of (12.5.1) into geometrical elements represented by the vortex panels. In Section 12.4, we discussed straight elements with linear strength distribution. In more advanced implementations, curved elements, such as sections of parabolas and circular arcs, and quadratic or higher-order strength density distributions are employed.

### Internal flow

Although the vortex sheet representation is physically meaningful only when it is applied to evaluate the stream function and velocity at a point in the flow, nothing prevents us from performing corresponding evaluations at a point inside the airfoil. When this is done, we find that the stream function is constant and the velocity vanishes inside the airfoil (Problem 12.5.2).

To explain this curiosity, we observe that the strength of the vortex sheet is computed to satisfy the no-penetration boundary condition around the airfoil. Because the normal component of the velocity is continuous across the vortex sheet, the interior flow occurs under vanishing normal boundary velocity. Since tangential velocity on the interior side of the airfoil is prohibited by the condition of irrotational motion in the absence of singular points, the fictitious internal flow must vanish.

### 12.5.1    Thin airfoil theory

Next, we consider flow past a thin cambered airfoil and introduce a system of coordinates such that the leading edge lies at the origin of the $x$ axis, and the trailing edge lies at the point $x = c$ along the $x$ axis, as illustrated in Figure 12.5.1. The camberline is described by the equation

$$y = \epsilon\, \eta_c(x), \tag{12.5.2}$$

where $\epsilon \ll 1$ is a small dimensionless number and $\eta_c(x)$ is the camberline shape function required to satisfy the geometrical constraints

$$\eta_c(0) = 0, \qquad \eta_c(c) = 0. \tag{12.5.3}$$

If $\eta_c(x) = 0$ for any $x$, the camberline is flat.

Because both sides of the airfoil are near the $x$ axis, the corresponding line integrals with respect to arc length in (12.5.1) can be approximated with integrals with respect to $x'$ from $x' = 0$ to $c$. Setting $y' = 0$, tracing the airfoil in the clockwise direction beginning from the trailing edge, and noting that on the upper side of the airfoil $d\ell' = dx'$ while on the lower side $d\ell' = -dx'$, we find that

$$\psi^{\text{vortex sheet}}(x, y) \simeq -\frac{1}{4\pi} \int_0^c \ln \frac{(x - x')^2 + y^2}{\varrho^2}\, (\gamma^+ - \gamma^-)(x')\, dx', \tag{12.5.4}$$
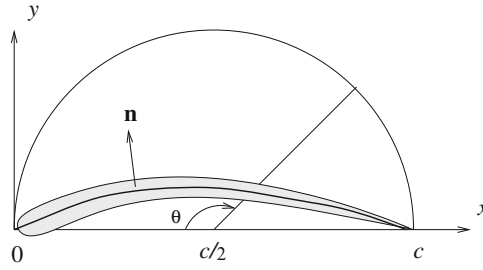
**Figure 12.5.1** Illustration of the camberline of a thin airfoil, and definition of variables used to develop the slender-airfoil theory.

where the superscripts + and - denote, respectively, the upper and lower side of the camberline. Defining

$$\chi \equiv \gamma^+ - \gamma^-, \tag{12.5.5}$$

we obtain a representation in terms of an effective flat vortex sheet extending between the leading and trailing edge,

$$\psi^{\text{vortex sheet}}(x, y) \simeq -\frac{1}{4\pi} \int_0^c \ln \frac{(x - x')^2 + y^2}{\varrho^2} \, \chi(x') \, \mathrm{d}x'. \tag{12.5.6}$$

The corresponding velocity potential is given by

$$\phi^{\text{vortex sheet}}(x, y) \simeq \frac{1}{2\pi} \int_0^c \arctan\left(\frac{y}{x - x'}\right) \chi(x') \, \mathrm{d}x'. \tag{12.5.7}$$

Our goal is to compute the strength of the effective vortex sheet, $\chi$, so as to satisfy the no-penetration condition around the airfoil.

*Velocity on either side of the vortex sheet*

As a preliminary, we consider the velocity induced by the effective vortex sheet on the upper and lower sides of the airfoil. To begin, we consider the limit of the velocity potential as the evaluation point, $\mathbf{x} = (x, y)$, approaches the vortex sheet from the upper side; that is, as $y \to 0_+$ with $0 < x < c$. In this limit, the inverse tangent function on the right-hand side of (12.5.7) is zero when $x' < x$, or $\pi$ when $x' > x$. Consequently, the potential takes the value

$$\phi^{\text{vortex sheet}}(x, y \to 0_+) = \tfrac{1}{2} \int_x^c \chi(x') \, \mathrm{d}x'. \tag{12.5.8}$$

Differentiating this expression with respect to $x$, we find that the $x$ velocity component is given by

$$u_x^{\text{vortex sheet}}(x, y \to 0_+) = -\tfrac{1}{2} \chi(x). \tag{12.5.9}$$

Working in a similar fashion for the lower side of the airfoil, we obtain

$$u_x^{\text{vortex sheet}}(x, y \to 0_-) = \tfrac{1}{2}\,\chi(x). \tag{12.5.10}$$

The last two equations illustrate once again that the velocity undergoes a discontinuity whose magnitude is equal to the strength of the vortex sheet.

The $y$ velocity component over the airfoil can be found by differentiating either the stream function given in (12.5.6) with respect to $x$ or the velocity potential given in (12.5.7) with respect to $y$. Either way, we find that

$$u_y^{\text{vortex sheet}}(x, y = 0_\pm) = \frac{1}{2\pi} \int_0^c \frac{\chi(x')}{x - x'}\,\mathrm{d}x'. \tag{12.5.11}$$

Unlike the $x$ velocity component, the $y$ velocity component remains continuous across the vortex sheet.

### Asymptotics

To compute the strength of the effective vortex sheet, $\chi$, we implement the no-penetration boundary condition through a series of approximations that may appear drastic but have a solid theoretical foundation.

First, we replace the disturbance flow due to the airfoil with the flow due to the effective vortex sheet expressed by (12.5.6) or (12.5.7). Enforcing the no-penetration boundary condition at the camberline, we obtain

$$\mathbf{n} \cdot \big(\mathbf{U} + \mathbf{u}^{\text{vortex sheet}}(y = \epsilon \eta_c)\big) = 0, \tag{12.5.12}$$

where $\mathbf{n}$ is the unit vector normal to the camberline on the upper side, pointing into the fluid. Using the geometrical representation (12.5.2), we find that

$$n_x = -\epsilon\,\frac{\eta_c'}{\sqrt{1 + \epsilon^2\,\eta_c'^2}}, \qquad n_y = \frac{1}{\sqrt{1 + \epsilon^2\,\eta_c'^2}}, \tag{12.5.13}$$

where $\eta_c' = \mathrm{d}\eta_c/\mathrm{d}x$. Because $\epsilon$ has been assumed small, the denominators can be replaced by unity, yielding the simplified expressions

$$n_x \simeq -\epsilon\,\frac{\mathrm{d}\eta_c}{\mathrm{d}x}, \qquad n_y \simeq 1. \tag{12.5.14}$$

A second approximation arises by replacing the velocity at the upper side of the camberline with the velocity at the upper side of the effective vortex sheet, given in (12.5.9) and (12.5.11).

Substituting (12.5.14), (12.5.9), and (12.5.11) into (12.5.12), we obtain

$$-\epsilon\,\frac{\mathrm{d}\eta_c}{\mathrm{d}x}\left(U_x - \tfrac{1}{2}\,\chi(x)\right) + U_y + \frac{1}{2\pi}\int_0^c \frac{\chi(x')}{x - x'}\,\mathrm{d}x' = 0. \tag{12.5.15}$$

Next, we confine our attention to flow that is nearly parallel to the $x$ axis, thereby assuming that $U_y$ is small compared to $U_x$. Writing

$$U_y = \tan \alpha \, U_x \simeq \alpha \, U_x, \tag{12.5.16}$$

we obtain

$$-\epsilon \left( \frac{\mathrm{d}\eta_c}{\mathrm{d}x} \right)_x \left( U_x - \tfrac{1}{2} \chi(x) \right) + \alpha \, U_x + \frac{1}{2\pi} \int_0^c \frac{\chi(x')}{x - x'} \, \mathrm{d}x' = 0, \tag{12.5.17}$$

where $\alpha$ is the angle of attack.

Inspecting the various terms on the left-hand side of equation (12.5.17), we find that the magnitude of $\chi$ is on the order of $\epsilon$ or $\alpha$, both of which have been assumed small. Since $\chi$ is negligible compared to $U_x$, it can be discarded from the expression enclosed by the large parentheses. Rearranging, we obtain an integral equation of the first kind for $\chi(x)$,

$$\frac{1}{2\pi} \int_0^c \frac{\chi(x')}{x - x'} \, \mathrm{d}x' = U_x \left( \epsilon \frac{\mathrm{d}\eta_c}{\mathrm{d}x} - \alpha \right) \tag{12.5.18}$$

for $0 < x < c$.

### Solution by Fourier expansions

One way to solve equation (12.5.18) is by expanding the unknown function $\chi$ in a Fourier series with respect to the angle $\theta$ varying between $0$ and $\pi$, defined such that

$$x = c \, \tfrac{1}{2} \, (1 - \cos \theta), \tag{12.5.19}$$

as illustrated in Figure 12.5.1. Differentiating, we obtain

$$\mathrm{d}x = c \, \tfrac{1}{2} \, \sin \theta \, \mathrm{d}\theta. \tag{12.5.20}$$

The Kutta–Joukowski condition requires that the strength of the vortex sheet vanishes at the trailing edge located at $\theta = \pi$. Wind tunnel measurements show that a high peak occurs at the leading edge located at $\theta = 0$. Based on these observations, we express $\chi$ as the sum of the singular function, $\cot \frac{\theta}{2}$, and a sine Fourier series in the form

$$\chi(\theta) = 2 \, U_x \left( a_0 \cot \frac{\theta}{2} + \sum_{n=1}^{\infty} a_n \sin(n\theta) \right), \tag{12.5.21}$$

where $a_n$ are Fourier coefficients. Substituting (12.5.19) and (12.5.21) into (12.5.18), we obtain the equation

$$\frac{1}{\pi} \int_0^\pi \frac{\sin \theta'}{\cos \theta' - \cos \theta} \left[ a_0 \cot \frac{\theta'}{2} + \sum_{n=1}^{\infty} a_n \sin(n\theta') \right] \mathrm{d}\theta' = \epsilon \frac{\mathrm{d}\eta_c}{\mathrm{d}x} - \alpha. \tag{12.5.22}$$

The integrals on the left-hand side of (12.5.22) can be evaluated with the help of standard tables. First, we write

$$\cot \frac{\theta'}{2} = \frac{1 + \cos \theta'}{\sin \theta'}, \tag{12.5.23}$$

and find that

$$\int_0^\pi \frac{\sin \theta'}{\cos \theta' - \cos \theta} \cot \frac{\theta'}{2} \, d\theta' = \int_0^\pi \frac{1 + \cos \theta'}{\cos \theta' - \cos \theta} \, d\theta' = \pi. \tag{12.5.24}$$

Second, we note that

$$\int_0^\pi \frac{\sin \theta'}{\cos \theta' - \cos \theta} \sin(n\theta') \, d\theta' = -\pi \cos(n\theta). \tag{12.5.25}$$

Substituting these results into (12.5.22), we derive a remarkably simple expression,

$$a_0 - \sum_{n=1}^\infty a_n \cos(i\theta) = \epsilon \frac{d\eta_c}{dx} - \alpha. \tag{12.5.26}$$

The left-hand side of (12.5.26) is the cosine Fourier expansion of the right-hand side with respect to $\theta$. Multiplying both sides by $\cos(m\theta)$, where $m$ is an integer, integrating with respect to $\theta$ from 0 to $\pi$, and using the identity

$$\int_0^\pi \cos(n\theta) \cos(m\theta) \, d\theta = \begin{cases} 0 & \text{if } n \neq m, \\ \pi & \text{if } n = m = 0, \\ \frac{1}{2}\pi & \text{if } n = m \neq 0, \end{cases} \tag{12.5.27}$$

we obtain

$$a_0 = -\alpha + \epsilon \frac{1}{\pi} \int_0^\pi \left(\frac{d\eta_c}{dx}\right)_{x(\theta)} d\theta, \qquad a_n = -\epsilon \frac{2}{\pi} \int_0^\pi \left(\frac{d\eta_c}{dx}\right)_{x(\theta)} \cos(n\theta) \, d\theta \tag{12.5.28}$$

for $i = n, 2, \dots$.

The camberline slope, $d\eta_c/dx$, can be expanded in a cosine Fourier series with respect to $\theta$,

$$\left(\frac{d\eta_c}{dx}\right)_{x(\theta)} = \frac{1}{2} b_0 + \sum_{n=1}^\infty b_n \cos(n\theta), \tag{12.5.29}$$

where $b_n$ are dimensionless Fourier coefficients given by

$$b_n = \frac{2}{\pi} \int_0^\pi \left(\frac{d\eta_c}{dx}\right)_{x(\theta)} \cos(n\theta) \, d\theta \tag{12.5.30}$$

for $n = 0, 1, \dots,$. Substituting the right-hand side of (12.5.29) into (12.5.26) and setting the sum of like Fourier coefficients to zero, we obtain

$$a_0 = -\alpha + \epsilon \frac{1}{2} b_0, \qquad a_n = -\epsilon \, b_n \tag{12.5.31}$$

for $n = 1, 2, \ldots$. These relations illustrate that only the leading coefficient, $a_0$, depends on the angle of attack, $\alpha$, while the rest of the coefficients are determined exclusively by the geometry of the camberline.

### Lift, lift coefficient, and lift slope

To compute the lift force per unit span exerted on the airfoil, we use the Kutta–Joukowski theorem expressed by equation (12.2.4), obtaining

$$L = -\rho\, U_x \int_0^c \chi(x)\, \mathrm{d}x. \tag{12.5.32}$$

or

$$L = -\rho\, c\, U_x\, \frac{1}{2} \int_0^\pi \chi(\theta)\, \sin\theta\, \mathrm{d}\theta. \tag{12.5.33}$$

Substituting the expansion (12.5.21) into the right-hand side, we obtain

$$L = -\rho\, c\, U_x^2 \int_0^\pi \left( a_0 \cot\frac{\theta}{2} + \sum_{n=1}^\infty a_n \sin(n\theta) \right) \sin\theta\, \mathrm{d}\theta. \tag{12.5.34}$$

Evaluating the integrals, we find that only two terms make a non-zero contribution, yielding the lift force

$$L = -\pi\rho\, c\, U_x^2 \left( a_0 + \tfrac{1}{2}\, a_1 \right). \tag{12.5.35}$$

Using (12.5.31), we find that

$$L = \pi\rho\, c \left( \alpha - \epsilon\, \tfrac{1}{2}\, (b_0 + b_1) \right). \tag{12.5.36}$$

The lift coefficient is

$$c_L \equiv \frac{L}{\frac{1}{2}\,\rho\, c\, U_x^2} = -2\pi\, (a_0 + \tfrac{1}{2}\, a_1) = 2\pi \left( \alpha - \epsilon\, \tfrac{1}{2}\, (b_0 + b_1) \right). \tag{12.5.37}$$

In practical aerodynamics, the performance of an airfoil is characterized by the lift slope, defined as the slope $\mathrm{d}c_L/\mathrm{d}\alpha$. Our analysis has shown that the lift slope of a thin airfoil is constant, equal to $2\pi$, independent of the camber.

### Pressure difference across the airfoil

The difference in the pressure on either side of the vortex sheet representing the airfoil,

$$\Delta p \equiv p(x, y \to 0_-) - p(x, y \to 0_+), \tag{12.5.38}$$

can by computed using Bernoulli's equation (6.4.18). Using expressions (12.5.9) and (12.5.10), we find that the velocity on the upper or lower side of the vortex sheet is, respectively, equal

to $U_x - \frac{1}{2}\chi$ and $U_x + \frac{1}{2}\chi$. Substituting these expressions in Bernoulli's equation for irrotational flow, we obtain

$$\Delta p = \left( p_\infty - \tfrac{1}{2}\rho\left(U_x + \tfrac{1}{2}\chi\right)^2 \right) - \left( p_\infty - \tfrac{1}{2}\rho\left(U_x - \tfrac{1}{2}\chi\right)^2 \right) = -\rho\, U_x\, \chi, \qquad (12.5.39)$$

which is consistent with expression (12.5.32) for the lift force.

*Pressure moment*

The moment of the pressure force with respect to the leading edge is expressed by the integral

$$M = -\int_0^c x\, \Delta p\, \mathrm{d}x. \qquad (12.5.40)$$

Substituting expression (12.5.39) for the pressure drop, we obtain

$$M = \rho\, U_x \int_0^c x\, \chi(x)\, \mathrm{d}x = \tfrac{1}{4}\,\rho\, U_x\, c^2 \int_0^\pi \chi(\theta)\,(1 - \cos\theta)\sin\theta\, \mathrm{d}\theta. \qquad (12.5.41)$$

Substituting expansion (12.5.21), we obtain

$$M = \tfrac{1}{2}\,\rho\, U_x^2\, c^2 \int_0^\pi \left( a_0 \cot\frac{\theta}{2} + \sum_{n=1}^\infty a_n \sin(n\theta) \right)(1 - \cos\theta)\sin\theta\, \mathrm{d}\theta. \qquad (12.5.42)$$

Evaluating the integrals, we find

$$M = \tfrac{1}{4}\,\pi\rho\, c^2\, U_x^2(a_0 + a_1 - \tfrac{1}{2}\, a_2), \qquad (12.5.43)$$

which shows that only three coefficients contribute to the pressure moment. The moment coefficient is defined as

$$c_M \equiv \frac{M}{\tfrac{1}{2}\,\rho\, c^2\, U_x^2} = \tfrac{1}{2}\,\pi\left(a_0 + a_1 - \tfrac{1}{2}\, a_2\right). \qquad (12.5.44)$$

The moment of the pressure forces with respect to an arbitrary point, $x = x_m$, is given by

$$M_{x_m} = -\int_o^c (x - x_m)\, \Delta p\, \mathrm{d}x = M + x_m\, L, \qquad (12.5.45)$$

where $L$ is the lift force. Substituting expressions (12.5.35) and (12.5.43) for $L$ and $M$ into the right-hand side of (12.5.45), we find that

$$M_{x_m} = \pi\rho\, c\, U_x^2 \left( \tfrac{1}{4}\, c\,(a_0 + a_1 - \tfrac{1}{2}\, a_2) - x_m\,(a_0 + \tfrac{1}{2}\, a_1) \right). \qquad (12.5.46)$$

When $x_m = \frac{1}{4}c$, the coefficient $a_0$ disappears from the right-hand side of (12.5.46) and the pressure moment becomes independent of the angle of attack, $\alpha$. The quarter chord moment, $M_{c/4}$,

$$M_{c/4} = \frac{1}{8} \pi \rho \, c^2 \, U_x^2 \, (a_1 - a_2), \qquad (12.5.47)$$

and associated moment coefficient,

$$c_{M_{c/4}} \equiv \frac{M_{c/4}}{\frac{1}{2} \rho \, c^2 \, U_x^2} = \frac{1}{4} \pi \, (a_1 - a_2), \qquad (12.5.48)$$

are used to characterize the performance of an airfoil.

### Symmetric airfoils

Since the camber of a symmetric airfoil vanishes, we may set $\epsilon = 0$ or $\eta_c(x) = 0$ in the preceding equations. Equations in (12.5.31) yield $a_0 = -\alpha$ and $a_n = 0$ for $n = 1, 2, \ldots$, and expansion (12.5.21) reduces to

$$\chi = -2 \, \alpha \, U_x \cot \frac{\theta}{2}. \qquad (12.5.49)$$

The lift force and lift coefficient computed from equations (12.5.35) and (12.5.37) are given by

$$L = \alpha \pi \rho \, c \, U_x^2, \qquad c_L = 2 \, \alpha \, \pi. \qquad (12.5.50)$$

The moment and moment coefficient computed from equations (12.5.43) and (12.5.44) are given by

$$M = -\alpha \pi \rho c^2 \, U_x^2, \qquad c_M = -\frac{\alpha}{2} \, \pi. \qquad (12.5.51)$$

### PROBLEMS

**12.5.1** *Thin airfoil with parabolic camber*

Consider a thin airfoil with parabolic camberline described by the shape function

$$\eta_c(x) = \frac{4}{c} \, x \, (c - x). \qquad (12.5.52)$$

The camber is equal to $\epsilon \, \eta_c(\frac{1}{2}c) = \epsilon c$. Show that the lift and moment coefficients are given by

$$c_L = 2\pi \, (\alpha + 2 \, \epsilon), \qquad c_M = -\frac{\pi}{2} \, (\alpha + 4\epsilon). \qquad (12.5.53)$$

Note that the lift vanishes when $\alpha = -2\epsilon$.

**12.5.2** *NACA 23012 airfoil*

The camberline of the NACA 23012 airfoil is described as

$$\widehat{y} = \begin{cases} 2.6595\,(\widehat{x}^3 - 0.6075\widehat{x}^2 + 0.1147\,\widehat{x}) & \text{for } 0 \le \widehat{x} \le 0.2025, \\ 0.02208\,(1 - \widehat{x}) & \text{for } 0.2025 \le \widehat{x} \le 1 \,, \end{cases} \tag{12.5.54}$$

where $\widehat{x} equiv x/c$ and $\widehat{y} \equiv y/c$. Derive expressions for the lift and moment coefficients in terms of the angle of attack. Compare your results with experimental measurements for $\alpha = 4°$, showing that $c_L = 0.55$ and $c_{M_{c/4}} = -0.01$.

**12.5.3** 🖳 *Comparison of asymptotics with the vortex panel method*

Consider the NACA 23012 airfoil discussed in Problem 12.5.2. Run the code *airf_2d_lvp* in directory *07_ptf* of FDLIB to compute the lift coefficient in wind axes. Compare the numerical results with the asymptotic predictions for small airfoil thickness.

## 12.6   Point-source-dipole panels

Consider the stream function of the flow induced by a vortex panel situated along the $x$ axis between the point $x = a$ and $b$, as shown in equation (12.3.8), repeated below for convenience,

$$\psi^{\text{vortex panel}}(x, y) = -\frac{1}{4\pi} \int_a^b \ln \frac{(x - x')^2 + (y - y')^2}{\varrho^2} \, \gamma(x') \, \mathrm{d}x', \tag{12.6.1}$$

with the understanding that $y' = 0$. The distribution of circulation along the panel, $\mu(x)$, is defined as the integral of the strength density of the vortex sheet with respect to $x$ from an arbitrary point $x = d \ge a$ up to an arbitrary point $x \le b$,

$$\mu(x) \equiv \int_d^x \gamma(x') \, \mathrm{d}x', \tag{12.6.2}$$

where $a \ge x \ge b$. Using the rules of integral differentiation, we find that

$$\frac{\mathrm{d}\mu}{\mathrm{d}x} = \gamma. \tag{12.6.3}$$

Substituting the left-hand side of (12.6.3) into the integral of (12.6.1), and integrating by parts, we obtain

$$\begin{aligned} \psi^{\text{vortex panel}}(x, y) = {} & \frac{\mu(x = a)}{2\pi} \ln \frac{(x - a)^2 + (y - y')^2}{\varrho^2} \\ & -\frac{\mu(x = b)}{2\pi} \ln \frac{(x - b)^2 + (y - y')^2}{\varrho^2} \\ & +\frac{1}{4\pi} \int_a^b \frac{\mathrm{d}}{\mathrm{d}x'} \Big( \ln \frac{(x - x')^2 + (y - y')^2}{\varrho^2} \Big) \mu(x') \, \mathrm{d}x', \end{aligned} \tag{12.6.4}$$

with the understanding that $y' = 0$ since the panel situated along the $x$ axis. Carrying out the differentiation under the integral sign, we derive the final form

$$\psi^{\text{vortex panel}}(x, y) = \frac{\mu(x = a)}{2\pi} \ln \frac{(x - a)^2 + (y - y')^2}{\varrho^2} \tag{12.6.5}$$

$$- \frac{\mu(x = b)}{2\pi} \ln \frac{(x - b)^2 + (y - y')^2}{\varrho^2} - \frac{1}{2\pi} \int_a^b \frac{x - x'}{(x - x')^2 + (y - y')^2} \, \mu(x') \, \mathrm{d}x'.$$

The three terms on the right-hand side of (12.6.5) admits the following interpretations:

- The first term represents the flow due to a point vortex with strength $-\mu(x = a)$ situated at the first panel end-point.

- The second term represents the flow due to a point vortex with strength $\mu(x = b)$ situated at the second panel end-point.

- Comparing the third term on the right-hand side of (12.6.5) with (3.5.38), we find that the third term represents the flow due to a distribution of point-source dipoles with strength density $\mu(x')$ oriented normal to the panel. If $\mu(x')$ is positive, the dipole at the point $x'$ is oriented toward the positive direction of the $y$ axis. If $\mu(x')$ is negative, the dipole at the variable point $x'$ is oriented toward the negative direction of the $y$ axis.

Now we introduce the stream function due to a point-source dipole panel,

$$\psi^{\text{source dipole panel}}(x, y) \equiv -\frac{1}{2\pi} \int_a^b \frac{x - x'}{(x - x')^2 + (y - y')^2} \, \mu(x') \, \mathrm{d}x', \tag{12.6.6}$$

and rearrange expression (12.6.5) to obtain

$$\psi^{\text{source dipole panel}}(x, y) = \psi^{\text{vortex panel}}(x, y) \tag{12.6.7}$$

$$= -\frac{\mu_a}{2\pi} \ln \frac{(x - a)^2 + (y - y')^2}{\varrho^2} + \frac{\mu_b}{2\pi} \ln \frac{(x - b)^2 + (y - y')^2}{\varrho^2},$$

where $\mu_a = \mu(x = a)$ and $\mu_b = \mu(x = b)$.

Equation (12.6.7) establishes a correspondence between the flow due to a source-dipole panel and the flow due to a vortex panel, subject to the differential relation (12.6.3). The first term on the right-hand side of (12.6.7) represents the flow due to a point vortex with strength $\mu_a$ placed at the first panel end-point, and the second term represents the flow due to a point vortex with strength $-\mu_b$ placed at the second panel end-point.

### Panels with uniform point-source dipole strength density

When the strength density of the source-dipole distribution is constant, $\mu = \mu_0$, the strength of the vortex sheet is identically zero and the first term on the right-hand side of (12.6.7) does not appears. In that case, the flow due to the panel is identical to the flow induced by two point vortices with strengths $\mu_0$ and $-\mu_0$ situated, respectively, at the first and second panel end-point.

### 12.6.1    *Source-dipole panel method*

The flow due to a point-source dipole panel can be used as a fundamental building block for representing and subsequently computing a flow of interest past an airfoil. To develop the source-dipole panel method, we work as with the vortex panel method discussed in Section 12.4, with some modifications. In the first step, we trace the contour of the airfoil with $N+1$ nodes distributed in the clockwise direction, as illustrated in Figure 12.4.1. A pair of successive nodes , $\mathbf{x}^{(i)}$ and $\mathbf{x}^{(i+1)}$, defines the $i$th flat source-dipole panel.

In the second step, the velocity at a point in the flow is described by a superposition of the incident flow and the flows induced by the $N$ source-dipole panels. An additional degree of freedom is required to specify the circulation around the airfoil. This degree of freedom is provided by an additional contribution mediated by a point vortex with strength $\kappa$ placed at the trailing edge. The composite representation is

$$\mathbf{u}(x,y) = \mathbf{U} + \sum_{i=1}^{N} \mathbf{u}^{(i)}(x,y) + \mathbf{u}^{\text{point vortex}}_{\text{at trailing edge}}(x,y), \tag{12.6.8}$$

where $\mathbf{u}^{(i)}(x,y)$ is the velocity induced by the $i$th panel.

#### Uniform panels

We have seen that, if the source-dipole strength is uniform over each panel, the flow induced by the $i$th panel is identical to the flow induced by two point vortices with strength $\mu^{(i)}$ and $-\mu^{(i)}$ located at the first or second panel end-point, where $\mu^{(i)}$ is the constant value of the source-dipole strength density over the panel. Consequently, the $i$th node for $i = 2,\ldots,N$ hosts two point-vortices. One point vortex with strength $-\mu^{(i-1)}$ is contributed by the $i-1$ panel, and a second point vortex with strength $\mu^{(i)}$ is contributed by the $i$ panel. The combined strength is $\mu^{(i)} - \mu^{(i-1)}$.

The first node, located at the trailing edge, hosts three point vortices: one due to the first panel labeled 1, a second due to the last panel labeled $N$, and a third circulation-producing point vortex placed at the trailing edge. The Kutta–Joukowski condition requires that the net strength of the trailing point vortex is zero,

$$\mu^{(1)} - \mu^{(N)} + \kappa = 0. \tag{12.6.9}$$

The $N+1$ unknowns, including $\mu^{(i)}$ for $i = 1,\ldots,N$ and $\kappa$, can be computed by the collocation method discussed in Section 12.3, incorporating the Kutta–Joukowski condition (12.6.9).

#### Linear panels

When the strength density of a source-dipole panel varies linearly with respect to arc length, all three terms on the right-hand side of (12.6.7) make a contribution to the induced velocity field. Expression (12.6.3) shows that the strength density of the equivalent vortex sheet is constant and equal to the slope of the dipole density over the panel.

    In the linear source-dipole panel method, the flow is represented by a superposition of the three constituents shown in equation (12.6.8), where the dipole density over the $i$th panel varies linearly with respect to arc length from the initial value $\mu^{(i)}$ to the final value $\mu^{(i+1)}$. Summing the flows due to the individual panels expressed by the right-hand side of (12.6.7), and consolidating the left- and right-panel point vortices at the panel end points, we derive an equivalent representation in terms of point vortices and vortex panels with constant strength. The uniform strength density of the $i$th corresponding vortex panel is

$$\gamma^{(i)} \equiv \frac{\mu^{(i+1)} - \mu^{(i)}}{\Delta\ell_i}, \tag{12.6.10}$$

where $\Delta\ell_i$ is $i$th the panel length.

    Because the dipole strength is continuous around the approximate polygonal contour of the airfoil described by the panels, the strength of the point vortices vanishes at all but the first point where it takes the value $\mu^{(1)} - \mu^{(N+1)} + \kappa$. We conclude that the linear source-dipole panel representation is equivalent to the uniform vortex panel representation supplemented by a point vortex at the trailing edge. The strength of the point vortex must vanish to satisfy the Kutta–Joukowski condition at the trailing edge, as required by equation (12.6.9).

### 12.6.2   *Source-dipole representation*

As the number of panels, $N$, increases, the individual panel strength density distributions join to yield a smooth distribution defined around the airfoil. Correspondingly, the sum on the right-hand side of (12.6.8) reduces to an integral with respect to arc length around the airfoil, yielding an integral representation in terms of a source-dipole sheet.

    Equation (12.6.7) provides us with an expression for the stream function associated with a source-dipole panel situated over the $x$ axis, where the source-dipoles point along the $y$ axis. Generalizing this expression, we find that the stream function associated with source-dipole distribution around the airfoil is given by

$$\psi^{\text{source dipole sheet}}(x,y) = -\frac{1}{2\pi} \oint \frac{(x-x')\,n_y(\mathbf{x}') - (y-y')\,n_x(\mathbf{x}')}{(x-x')^2 + (y-y')^2}\,\mu(\mathbf{x}')\,\mathrm{d}\ell', \tag{12.6.11}$$

where $\mathrm{d}\ell' = (\mathrm{d}x'^2 + \mathrm{d}y'^2)^{1/2}$ is the differential arc length around the airfoil measured in the clockwise direction from a designated origin. The associated velocity potential is

$$\phi^{\text{source dipole sheet}}(x,y) = -\frac{1}{2\pi} \oint \frac{(x-x')\,n_x(\mathbf{x}') + (y-y')\,n_y(\mathbf{x}')}{(x-x')^2 + (y-y')^2}\,\mu(\mathbf{x}')\,\mathrm{d}\ell'. \tag{12.6.12}$$

    The counterpart of the panel representation (12.6.8) is

$$\mathbf{u}(x,y) = \mathbf{U} + \mathbf{u}^{\text{source dipole sheet}}(x,y) + \mathbf{u}^{\text{point vortex}}_{\text{at trailing edge}}(x,y), \tag{12.6.13}$$

where the second term on the right-hand side is the velocity corresponding to the stream function (12.6.11) and velocity potential (12.6.12). The stream function and velocity potential are given by the corresponding expressions

$$\psi(x,y) = U_x y - U_y x + \psi^{\text{source dipole sheet}}(x,y) + \psi^{\text{point vortex}}_{\text{at trailing edge}}(x,y), \qquad (12.6.14)$$

and

$$\phi(x,y) = U_x x + U_y y + \phi^{\text{source dipole sheet}}(x,y) + \phi^{\text{point vortex}}_{\text{at trailing edge}}(x,y). \qquad (12.6.15)$$

Conversely, the source-dipole panel representation arises from the discretization the integral on the right-hand side of (12.6.11) or (12.6.12) into geometrical elements representing source-dipole panels. In this section, we have discussed straight elements with constant and linear strength density distributions. In more advanced implementations, curved elements, such as sections of a parabola and circular arcs, and quadratic or higher-order strength density distributions are employed.

### 12.6.3   *Solution of the interior problem*

Assume that the strength of the source-dipole sheet is available such that the no-penetration condition around the airfoil is satisfied. For reasons discussed in Section 12.3, if we evaluate the right-hand sides of equations (12.6.11)–(12.6.13) at a point located inside the airfoil, we will find that the velocity vanishes and the stream function and potential take constant values. This observation suggests an alternative method of computing the strength density of the source dipoles. Instead of using the Neumann no-penetration boundary condition, we can use the Dirichlet boundary condition requiring that the potential and stream function are constant along the *interior* side of the airfoil.

*Panels with constant strength density*

To illustrate the implementation of the method, we discretize the airfoil contour into $N$ flat panels with constant strength density, as illustrated in Figure 12.4.1. Identifying the flow induced by each panel with the flow induced by two point vortices located at the panel end-points, as discussed earlier in this section, we obtain the potential

$$\phi(x,y) = U_x\,x + U_y\,y + \frac{1}{2\pi}\sum_{i=1}^{N}\left[\mu^{(i)}(\theta_1^{(i)} - \theta_2^{(i)})\right] + \frac{\kappa}{2\pi}\,\theta_{\text{T}}, \qquad (12.6.16)$$

where $\kappa$ is the strength of the point vortex at the trailing edge, and the angles $\theta_1^{(i)}$, $\theta_2^{(i)}$, and $\theta_{\text{T}}$ are defined in Figure 12.4.1.

To implement the collocation method, we evaluate (12.6.16) at the mid-point of the $j$th panel, $(x_{\text{M}}^{(j)}, y_{\text{M}}^{(j)})$, on the interior side of the airfoil for $j = 1,\ldots,N$. Next, we note that $\theta_1^{(j)} = 0$ and $\theta_2^{(j)} = -\pi$, and assign to the potential the reference value of zero to derive an

algebraic equation,

$$0 = U_x\, x_{\mathrm{M}}^{(j)} + U_y\, y_{\mathrm{M}}^{(j)} + \frac{1}{2\pi} \sum_{i=1}^{N} {}' \left[ \mu^{(i)}(\theta_1^{(i)} - \theta_2^{(i)}) \right] + \tfrac{1}{2}\, \mu^{(j+1)} + \frac{\kappa}{2\pi}\, \theta_{\mathrm{T}}, \qquad (12.6.17)$$

where the prime after the summation symbol denotes that the term $i = j$ is excluded from the sum. Rearranging (12.6.17), we derive a linear equation relating the panel source-dipole densities to the strength of the trailing-edge point vortex,

$$\tfrac{1}{2}\, \mu^{(j+1)} + \frac{1}{2\pi} \sum_{i=1}^{N} {}' \left[ \mu^{(i)}(\theta_1^{(i)} - \theta_2^{(i)}) \right] + \frac{\kappa}{2\pi}\, \theta_{\mathrm{T}} = -U_x\, x_{\mathrm{M}}^{(j)} - U_y\, y_{\mathrm{M}}^{(j)}. \qquad (12.6.18)$$

Applying this equation for $j = 1, \ldots N$, and appending to the resulting system of equations the Kutta–Joukowski condition expressed by (12.6.9), we obtain a linear system for the $N + 1$ unknowns $\mu^{(i)}$ for $i = 1, \ldots N$, and $\kappa$.

### Distribution of the potential over the airfoil

Inspecting the third term on the right-hand side of (12.6.16) involving the sum, we find that the potential undergoes a discontinuity of magnitude $-\mu^{(i)}$ across the $i$th panel. Since the potential inside the airfoil is constant and equal to zero, the potential on the exterior side of the panel must be equal to $-\mu^{(i)}$.

This result applies in a more general context: the potential at the outer side of the airfoil is equal to the negative of the strength density of the source dipole. The tangential velocity may then be computed by numerically differentiating $\mu$ with respect to arc length around the airfoil.

### PROBLEM

**12.6.1** ▣ *Constant strength dipole panels*

Code *airf_2d_cdp,* located inside directory *07_ptf* of FDLIB, computes flow past an airfoil using the constant strength source-dipole-panel method.

(*a*) Run the code for an airfoil of your choice. Prepare graphs, and discuss the distribution of the pressure coefficient.

(*b*) Evaluate the velocity at several points inside the airfoil and discuss the results.

## 12.7 Point-source panels and Green's third identity

Previously in this chapter, we discussed flow representations in terms of vortex panels and point-source dipole panels expressed, respectively, by equations (12.5.1) and (12.6.12) or (12.6.13). In this section, we introduce a new representation in terms of distributions of point sources. Working by analogy with (12.6.13), we find that the harmonic potential of

the induced flow is given by

$$\phi^{\text{source distribution}}(x, y) = \frac{1}{4\pi} \oint \ln \frac{(x - x')^2 + (y - y')^2}{\varrho^2} \, \sigma(\mathbf{x}') \, \mathrm{d}\ell(\mathbf{x}'), \qquad (12.7.1)$$

where $\sigma(\mathbf{x})$ is the strength density of the distribution and $\varrho$ is an arbitrary reference length.

The point-source representation carries an important restriction: conservation of mass requires that the total strength of the point sources, defined as the integral of the strength density, $\sigma$, with respect to arc length around the airfoil, $\ell$, is zero. If this condition is not met, a net radial flow due to an effective point source will be established. This restriction is satisfied automatically only in the case of symmetric flow past a symmetric non-lifting airfoil at zero angle of attack, and in the absence circulatory motion.

In spite of this limitation, the point-source representation is not without its merits. Its usefulness stems predominantly from Green's third identity discussed in Section 12.7.2, stating that a judicious combination of the point source and source-dipole representation ensures the satisfaction of the zero flow rate condition, and also endows the strength densities of the distributions with simple and appealing physical interpretations.

### 12.7.1   *Source panels with constant density*

Consider a flat source panel with uniform strength density equal to $\sigma^{(0)}$ situated along the $x$ axis between the points $x = a$ and $b$. Applying (12.7.1) with $y' = 0$, we find that the corresponding velocity potential is given by

$$\phi^{(0)}(x, y) = \sigma^{(0)} \frac{1}{4\pi} \int_a^b \ln \frac{(x - x')^2 + y^2}{\varrho^2} \, \mathrm{d}x'. \qquad (12.7.2)$$

Note that this expression is identical to that for the stream function due to a vortex panel with constant strength density given in equation (12.3.11), subject to the substitution

$$\gamma^{(0)} = -\sigma^{(0)}. \qquad (12.7.3)$$

Referring to (12.3.12), we find that

$$\begin{aligned}
\phi^{(0)}(x, y) = \sigma^{(0)} \frac{1}{4\pi} \Big( &-(x - b) \ln \frac{(x - b)^2 + y^2}{\varrho^2} \\
&+ (x - a) \ln \frac{(x - a)^2 + y^2}{\varrho^2} \\
&+ 2y \big( \arctan \frac{y}{x - b} - \arctan \frac{y}{x - a} \big) - 2(b - a) \Big).
\end{aligned} \qquad (12.7.4)$$

The components of the velocity are found by straightforward differentiation, and are given by

$$u_x^{(0)}(x, y) = \frac{\partial \phi^{(0)}}{\partial x} = -\sigma^{(0)} \frac{1}{4\pi} \ln \frac{(x - b)^2 + y^2}{(x - a)^2 + y^2}, \qquad (12.7.5)$$
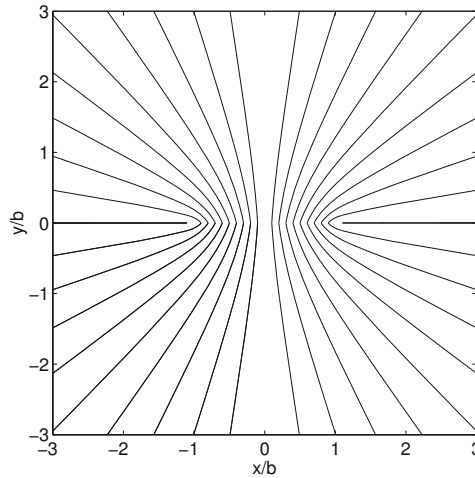
**Figure 12.7.1** Streamline pattern of the flow due to a point-source panel with uniform strength extending between the points $x = \pm b$.

and

$$u_y^{(0)}(x,y) = \frac{\partial \phi^{(0)}}{\partial y} = \sigma^{(0)} \frac{1}{2\pi} \left( \arctan \frac{y}{x-b} - \arctan \frac{y}{x-a} \right). \tag{12.7.6}$$

Far from the panel, the flow resembles that due to a point source with strength $m = \sigma^{(0)}(b-a)$ situated at the origin. The streamline pattern of the flow induced by a uniform panel extending between $x = \pm b$ is shown in Figure 12.7.1.

### Jump in the velocity across the panel

Expression (12.7.5) shows that the $x$ velocity component is continuous throughout the domain of flow and across the source panel. In contrast, because of the inverse tangent functions on the right-hand side of (12.7.6), the $y$ velocity component undergoes a discontinuity with magnitude $\sigma^{(0)}$ across the source panel. Specifically, the $y$ velocity component at the upper or lower side of the panel, $a < x < b$, is given by

$$u_y^{(0)}(x, y \to \pm 0) = \pm \tfrac{1}{2} \sigma^{(0)}. \tag{12.7.7}$$

Inverse tangent functions also appear on the right-hand side of (12.7.4). However, because these functions are multiplied by $y$, which is zero over the panel, a discontinuity in the potential does not arise.

### 12.7.2 Green's third identity

The source panels can be used in the familiar way to develop a representation of potential flow past a symmetric airfoil at zero angle of attack in the absence of circulation. The
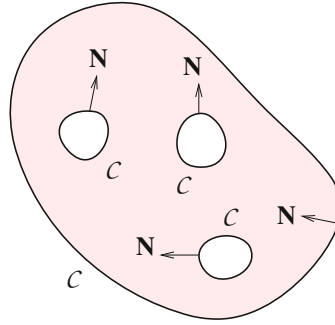
**Figure 12.7.2**   A control area in the $xy$ plane confined by a collection of closed contours, $\mathcal{C}$, is used to establish Green's third identity; $\mathbf{N}$ is the unit vector normal to the boundaries pointing into the fluid.

numerical implementation is analogous to that of the vortex panel method discussed in Section 12.3. However, a more interesting and more general representation is possible thanks to Green's third identity.

Consider a control area in the $xy$ plane enclosed by a collection of boundaries identified as closed contours, denoted by $\mathcal{C}$, as illustrated in Figure 12.7.2. Green's third identity states that the harmonic potential at a point $\mathbf{x}$ that lies inside the control area can be represented in terms of a combined point-source/source-dipole distribution, in the form

$$\phi(x, y) = \frac{1}{4\pi} \oint_{\mathcal{C}} \ln \frac{(x - x')^2 + (y - y')^2}{\varrho^2} \, \mathbf{N}(\mathbf{x}') \cdot \boldsymbol{\nabla}\phi(\mathbf{x}') \, \mathrm{d}\ell'$$

$$+ \frac{1}{2\pi} \oint_{\mathcal{C}} \frac{(x - x') \, N_x(\mathbf{x}') + (y - y') \, N_y(\mathbf{x}')}{(x - x')^2 + (y - y')^2} \, \phi(\mathbf{x}') \, \mathrm{d}\ell', \qquad (12.7.8)$$

where $\varrho$ is an arbitrary constant length and $\mathbf{N}$ is the unit vector normal to the boundaries pointing into the control area, as shown in Figure 12.7.2.

Comparing the two terms on the right-hand side of (12.7.8) with the representations (12.7.1) and (12.6.12), we identify the strength density of the point-source distribution with the boundary values of the potential, and the strength density of the source-dipole distribution with the boundary values of the normal derivative of the potential.

Next, we identify the control area with the area occupied by an airfoil, and apply Green's identity for the potential of an incident streaming flow, $\phi^{\infty}$. Writing $\mathbf{N} = -\mathbf{n}$, where $\mathbf{n}$ is the unit vector normal to the airfoil pointing into the *exterior* and $\mathbf{N}$ is the unit vector normal to the airfoil pointing into the *interior*, we obtain the representation

$$\phi_{\infty}(x, y) = -\frac{1}{4\pi} \oint_{\mathcal{C}} \ln \frac{(x - x')^2 + (y - y')^2}{\varrho^2} \, \mathbf{n}(\mathbf{x}') \cdot \boldsymbol{\nabla}\phi_{\infty}(\mathbf{x}') \, \mathrm{d}\ell'$$

$$-\frac{1}{2\pi} \oint_{\mathcal{C}} \frac{(x - x')\, n_x(\mathbf{x}') + (y - y')\, n_y(\mathbf{x}')}{(x - x')^2 + (y - y')^2}\, \phi_\infty(\mathbf{x}')\, d\ell', \tag{12.7.9}$$

where the point $\mathbf{x} = (x, y)$ lies inside the airfoil. Note the opposite signs on the right-hand sides of (12.7.8) and (12.7.9)

Equations (12.6.12) and (12.6.15) provide us a double-layer representation of the flow inside the airfoil in the form

$$\phi(x, y) = \phi_\infty(x, y) + \frac{1}{2\pi} \oint_C \frac{(x - x')\, n_x(\mathbf{x}') + (y - y')\, n_y(\mathbf{x}')}{(x - x')^2 + (y - y')^2}\, \phi^{(+)}(\mathbf{x}')\, d\ell'$$

$$+\phi^{\text{point vortex}}_{\text{at the trailing edge}}(x, y), \tag{12.7.10}$$

where $\phi^{(+)}$ is the potential on the exterior side of the airfoil. Since the point $\mathbf{x} = (x, y)$ is located in the interior of the airfoil, the left-hand side is a constant that may be set equal to zero.

Combining equations (12.7.9) and (12.7.10), we obtain

$$\frac{1}{4\pi} \oint_{\mathcal{C}} \ln \frac{(x - x')^2 + (y - y')^2}{\varrho^2}\, \mathbf{n}(\mathbf{x}') \cdot \boldsymbol{\nabla} \phi_\infty(\mathbf{x}')\, d\ell'$$

$$\tag{12.7.11}$$

$$= -\frac{1}{2\pi} \oint \frac{(x - x')\, n_x(\mathbf{x}') + (y - y')\, n_y(\mathbf{x}')}{(x - x')^2 + (y - y')^2}\, \mu(\mathbf{x}')\, d\ell' + \phi^{\text{point vortex}}_{\text{at the trailing edge}}(x, y),$$

where

$$\mu \equiv -\phi^{(+)} + \phi_\infty. \tag{12.7.12}$$

Equation (12.7.11) is an integral equation for the dipole density $\mu$. Once this equation has been solved using, for example, a panel method, the potential on the exterior side of the airfoil can be computed from equation (12.7.12) as

$$\phi^{(+)} = \phi_\infty - \mu. \tag{12.7.13}$$

The advantages of this representation over the vortex panel representation are now apparent.

## PROBLEMS

### 12.7.1 ▣ *Source-dipole panel method*

Program *airf_2d_csdp,* located in directory *07_ptf* of FDLIB, computes flow past an airfoil using a panel method based on equation (12.7.11). Run the code for an airfoil of your choice, prepare graphs and discuss the distribution of the pressure coefficient around the airfoil.

### 12.7.2 ▣ *Constant source panel method*

Write a code that computes flow past a symmetric airfoil at zero angle of attack using the point-source panel method. Run the code for an airfoil of your choice, prepare graphs, and discuss the distribution of the pressure coefficient around the airfoil.